Resolving the Physics of Relaxation: Flows, Reconnection, Heating, EUV bursts, and Waves

M. Haw, K. B. Chai, X. Zhai, and P. M. Bellan
California Institute of Technology

Relaxation as a dynamic cascade

Double Coronal Loop Experiment

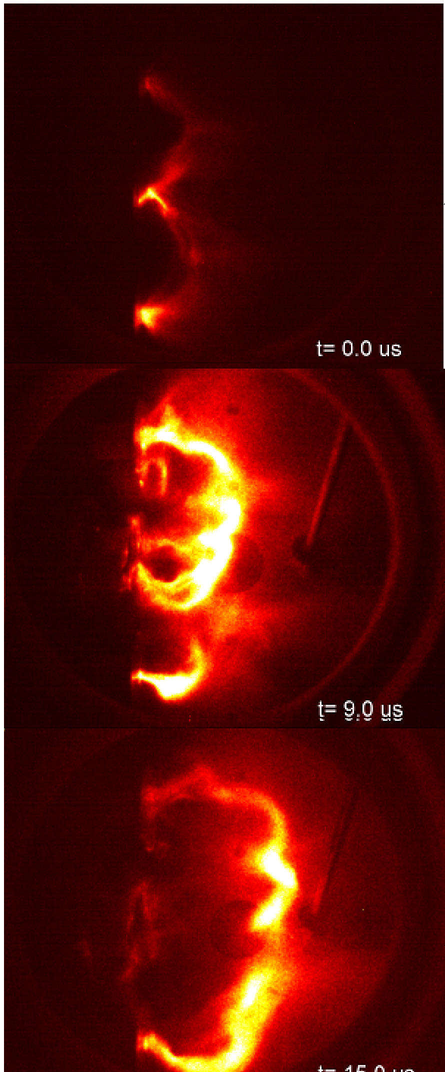

Astrophysical Jet Experiment

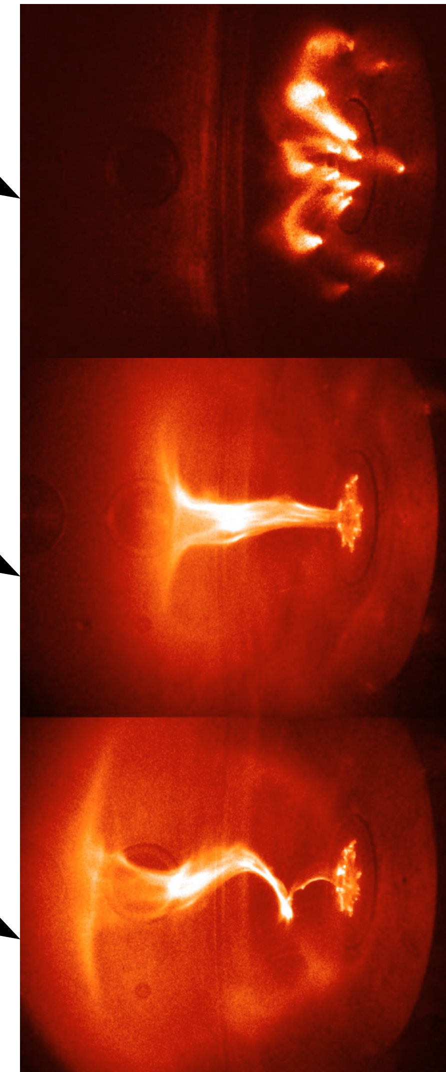

Helicity Injection

Nontrivial Boundary Conditions

mass flux, B-field, E-field

Flows and Collimation

Finite beta

Non-equilibrium evolution

Kink and Secondary Instabilities

Hall Reconnection
Wave coupling
Nonthermal heating

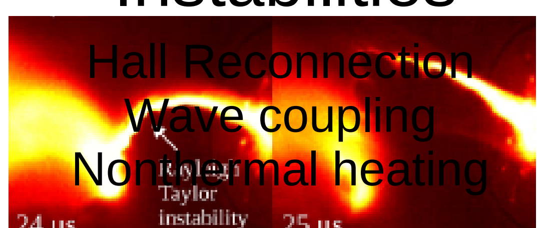

Double Solar Loop Experiment

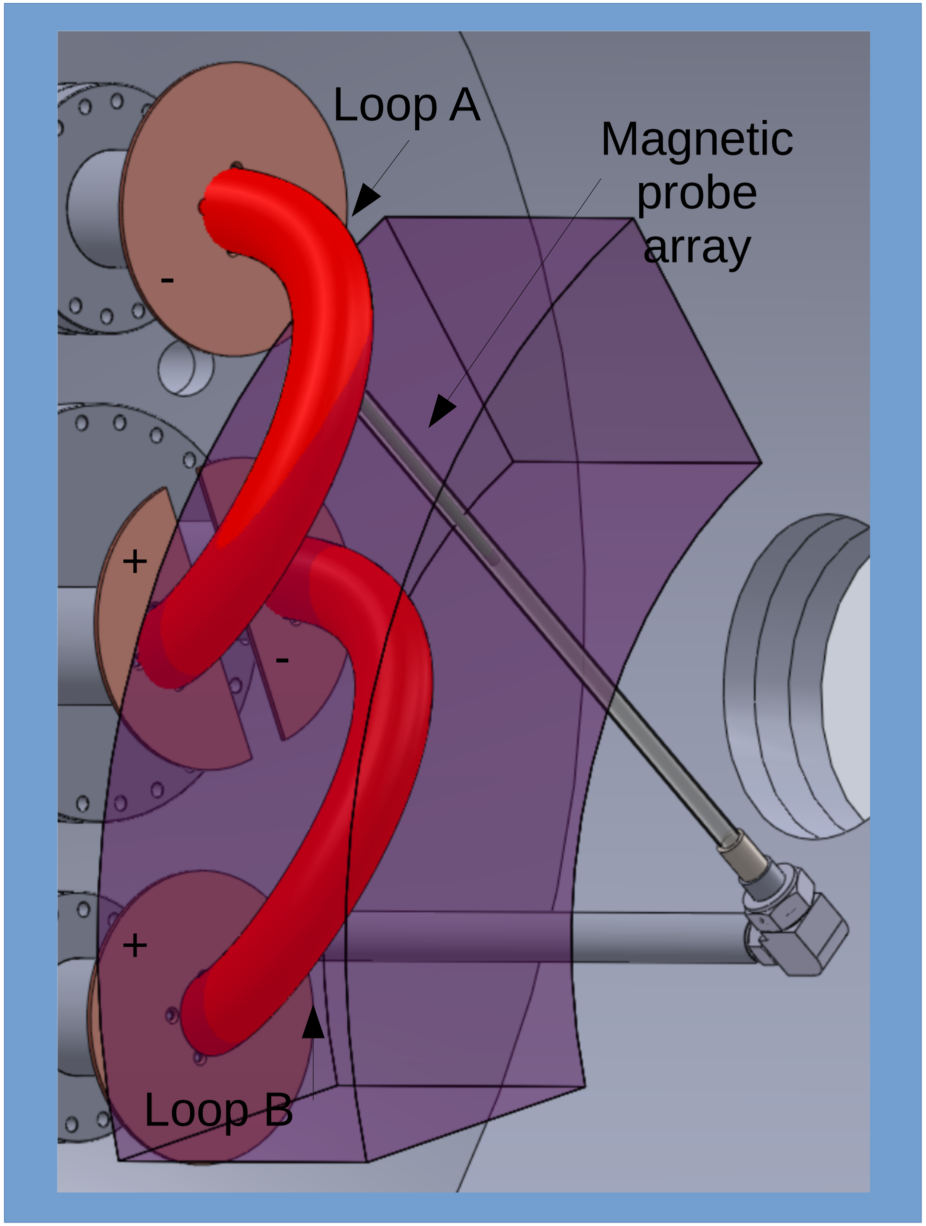

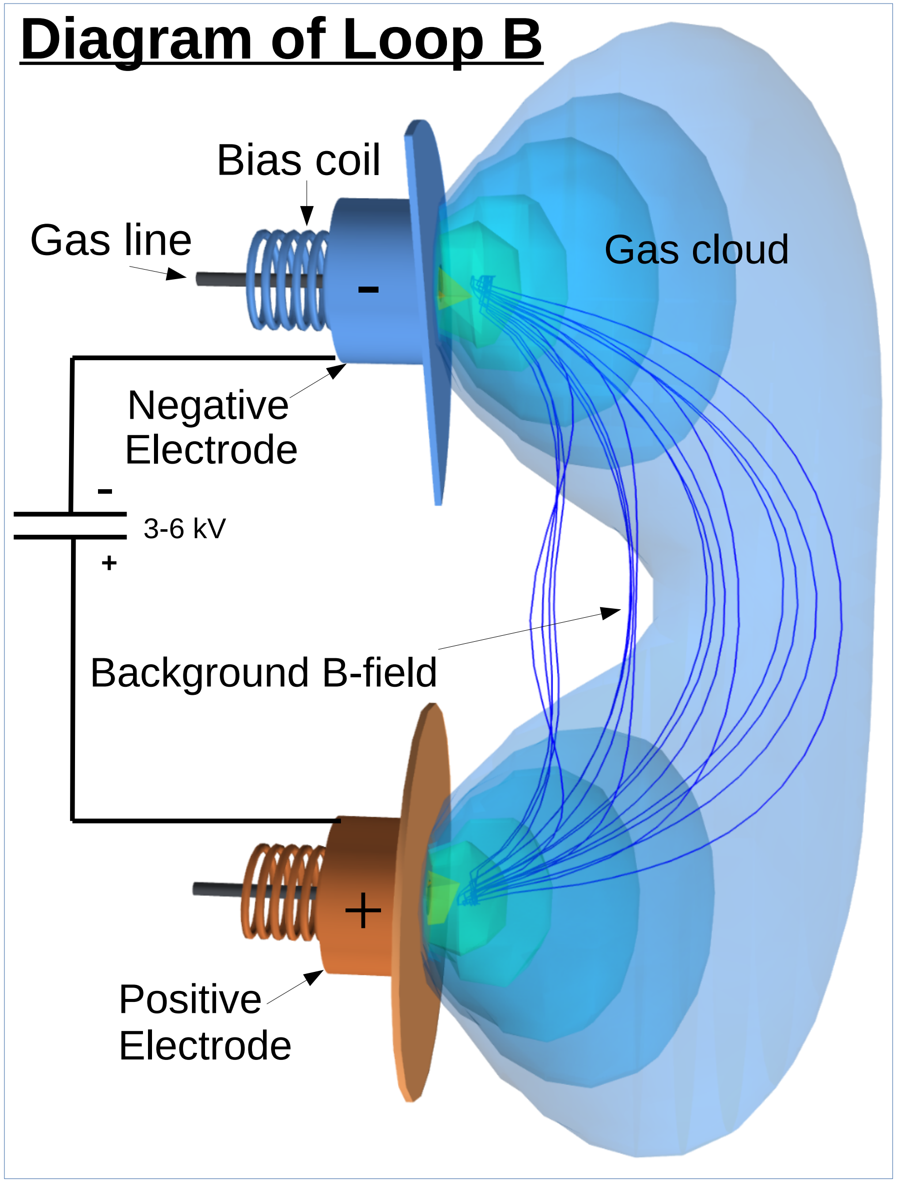

3D B-field Measurements

Vector B-field measured at 2700 positions with ~2cm spatial resolution

15 θ-positions, 10 z-positions
5 shots per position
Set of 750 shots

3D B-Field: 5-shots, high reproducibility

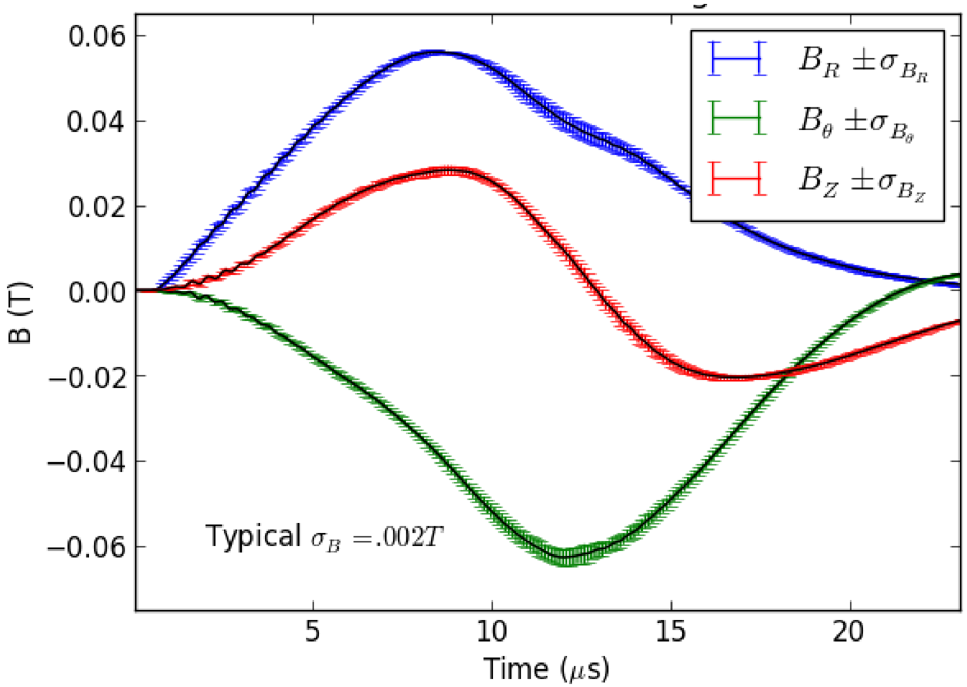

3D Measurement Volume

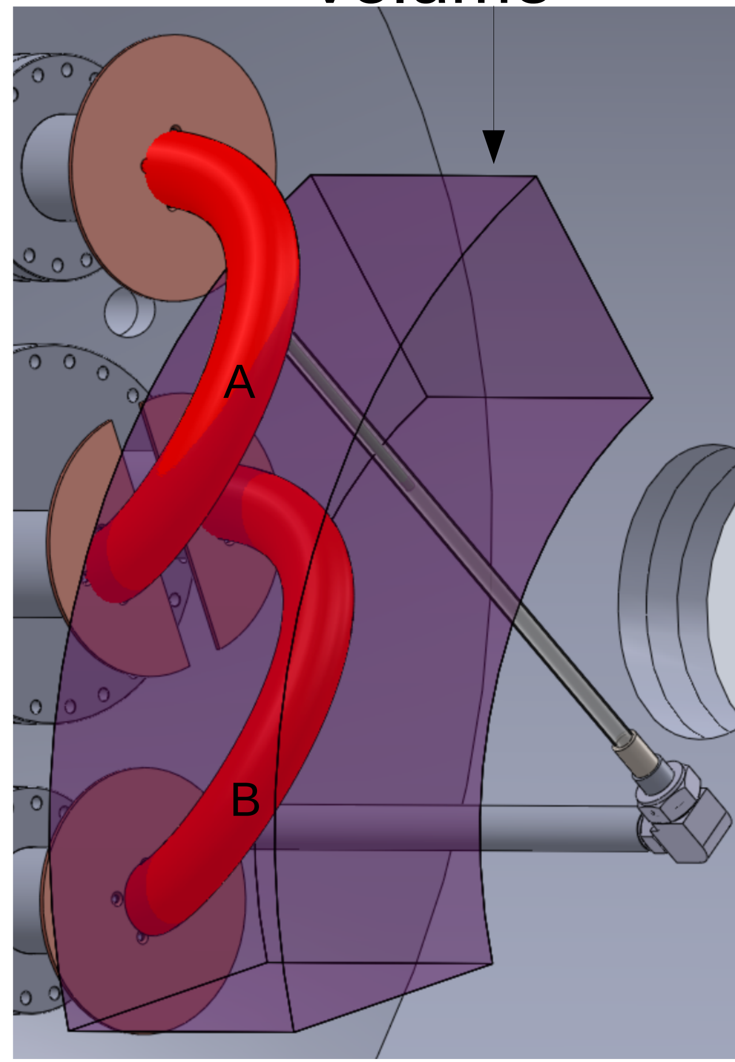

3D Laboratory Vector Measurements of B and J

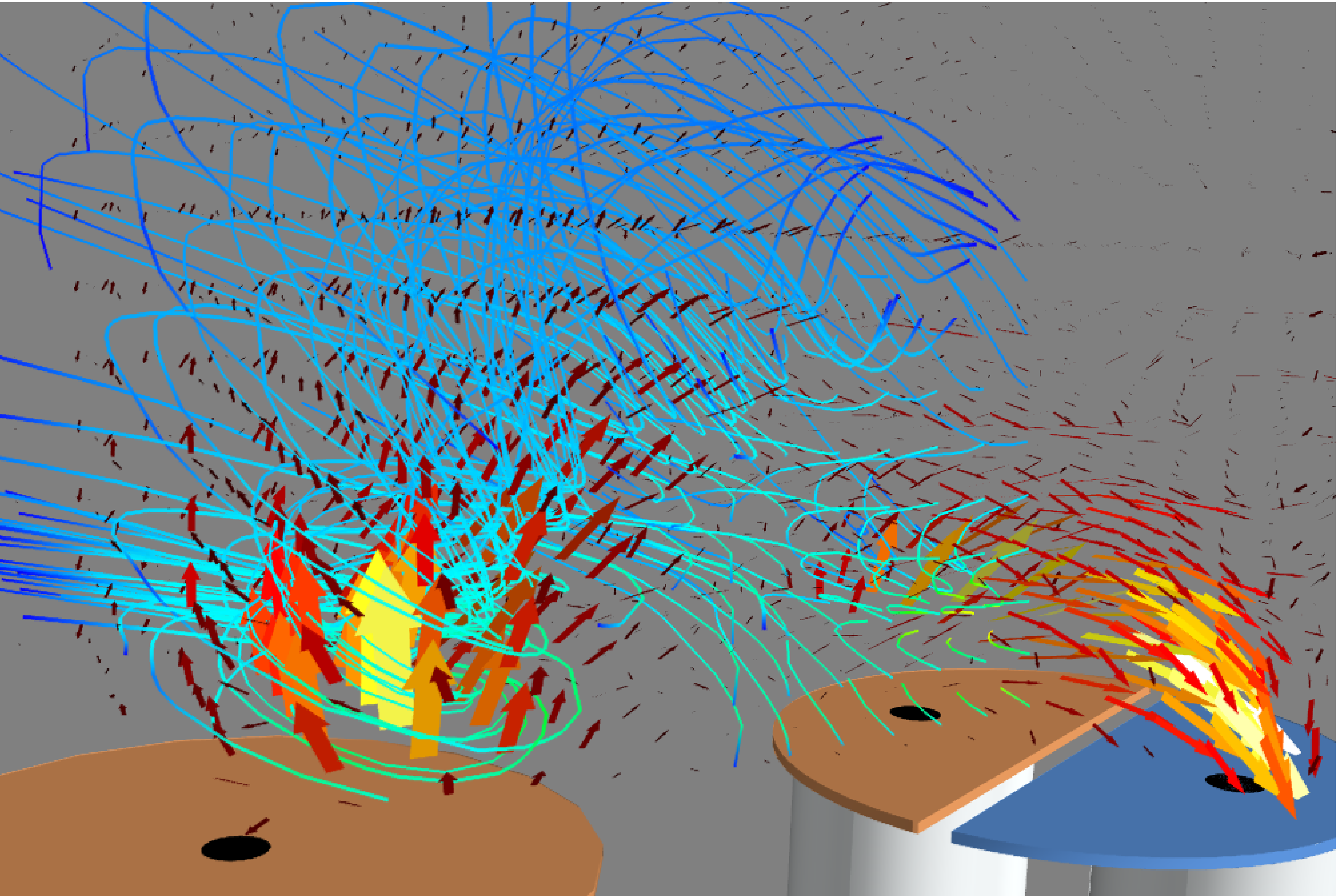

Validation of Probe Current Density

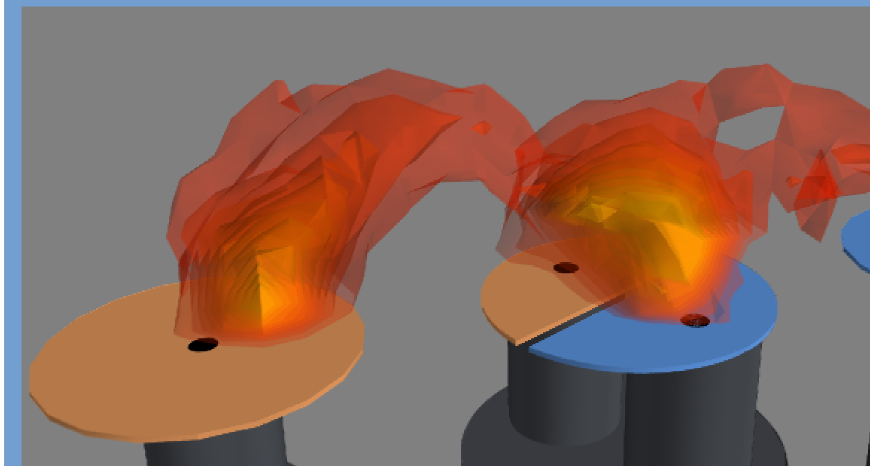

3D Current |J| isosurfaces from probe

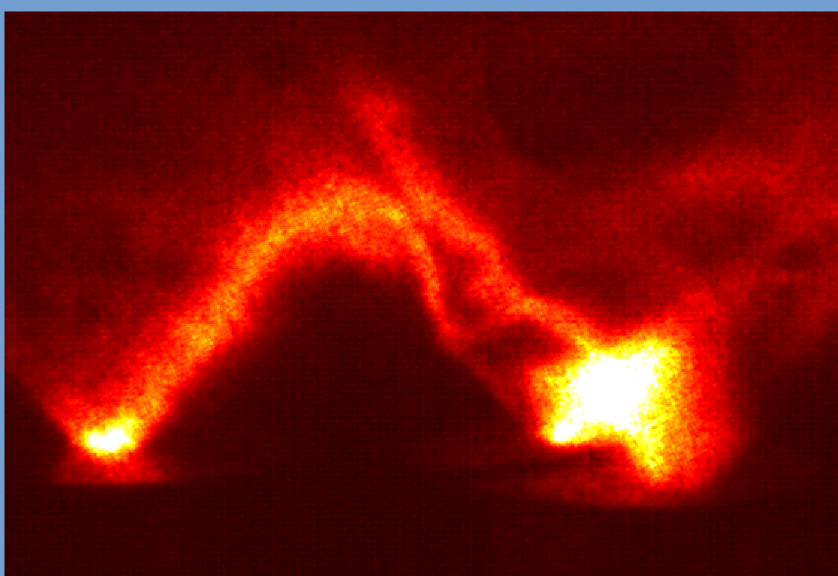

Image of plasma loops

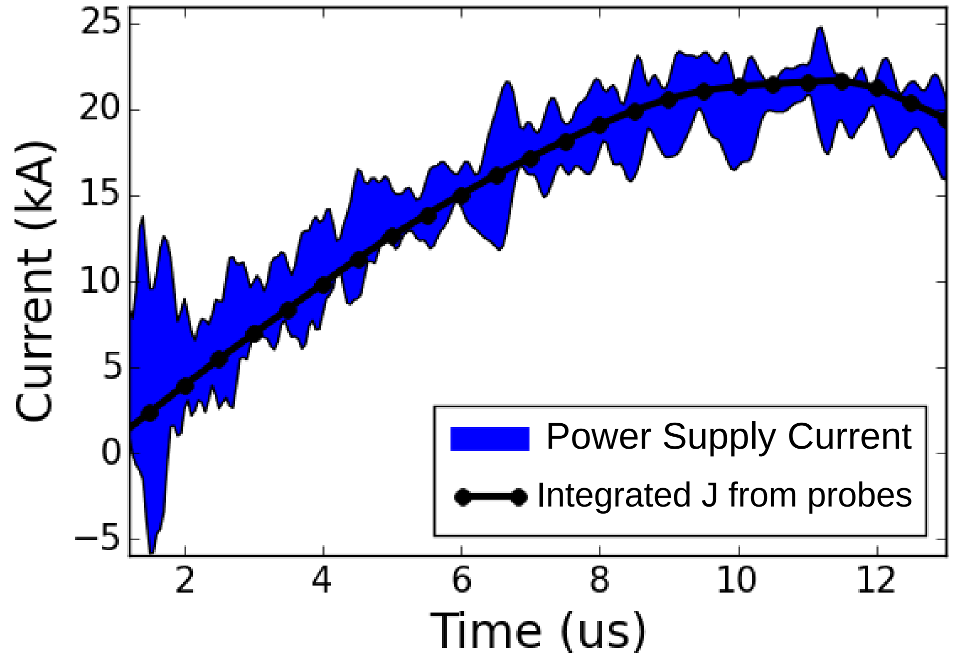

<u>Probe B-field measurements are sufficient to calculate J and therefore JxB force</u>

3D JxB Force Vectors

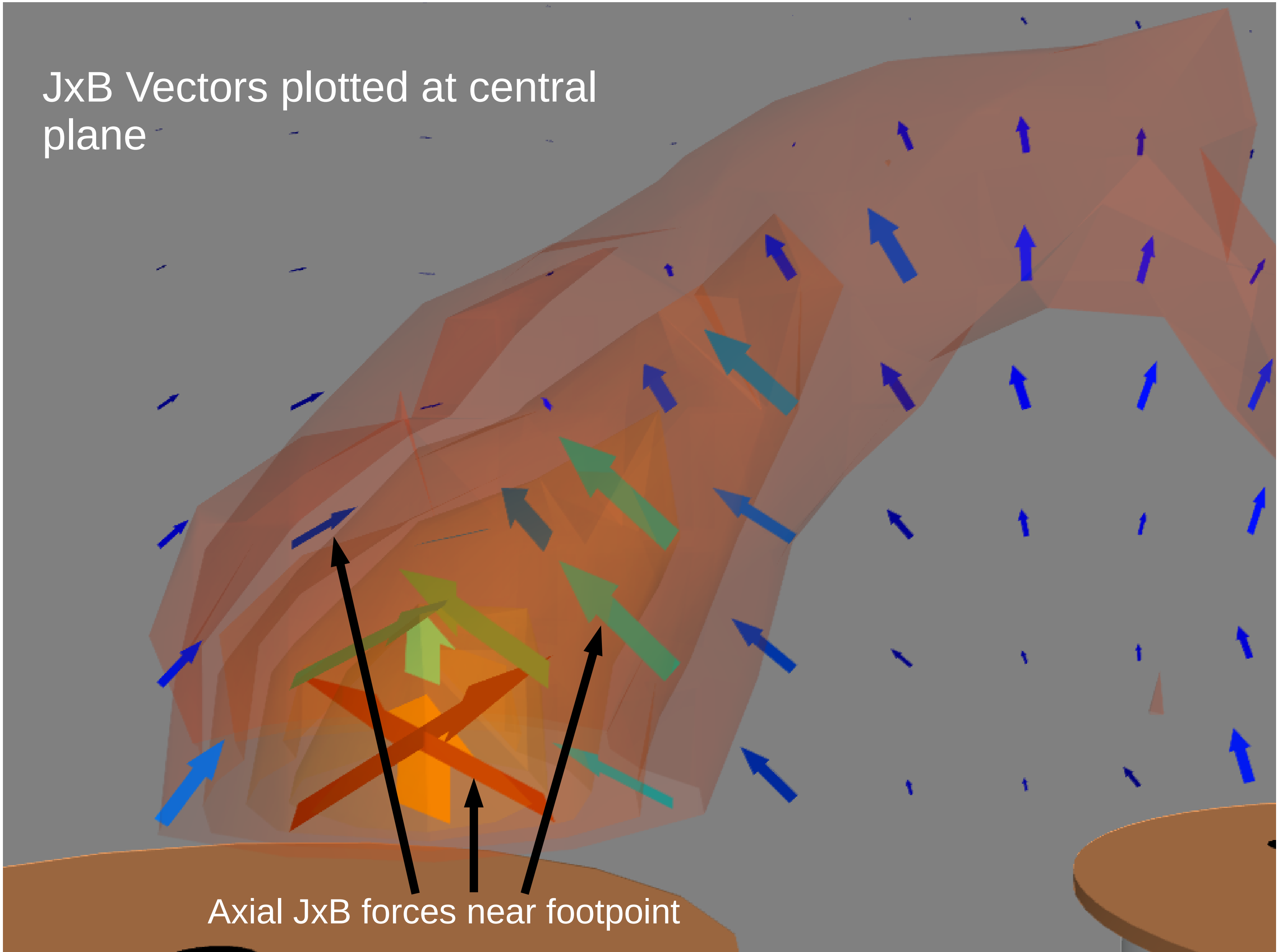

Axial cross-sections

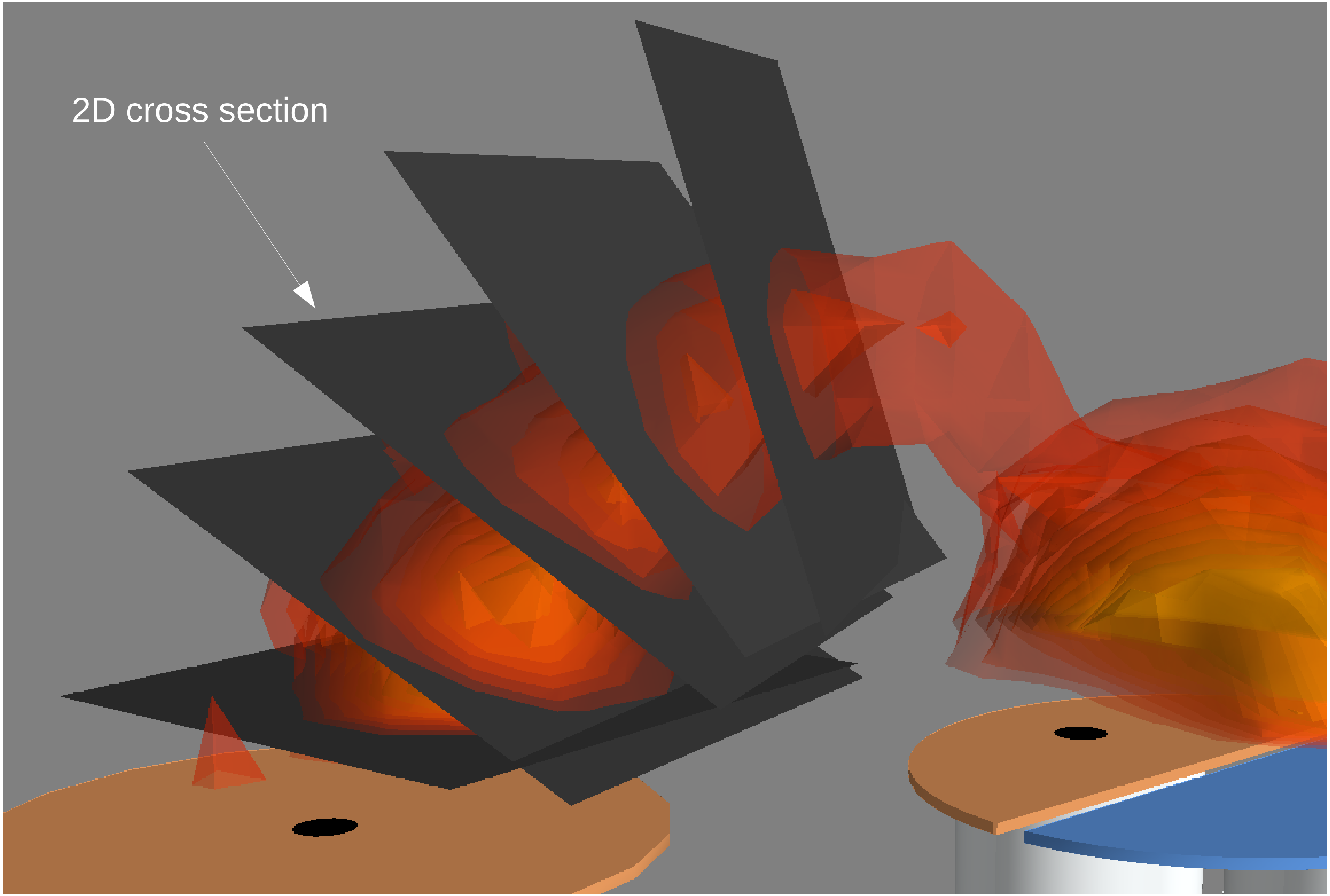

- To compare with theory, we extract cross-sections along the axis

Force cross-sections

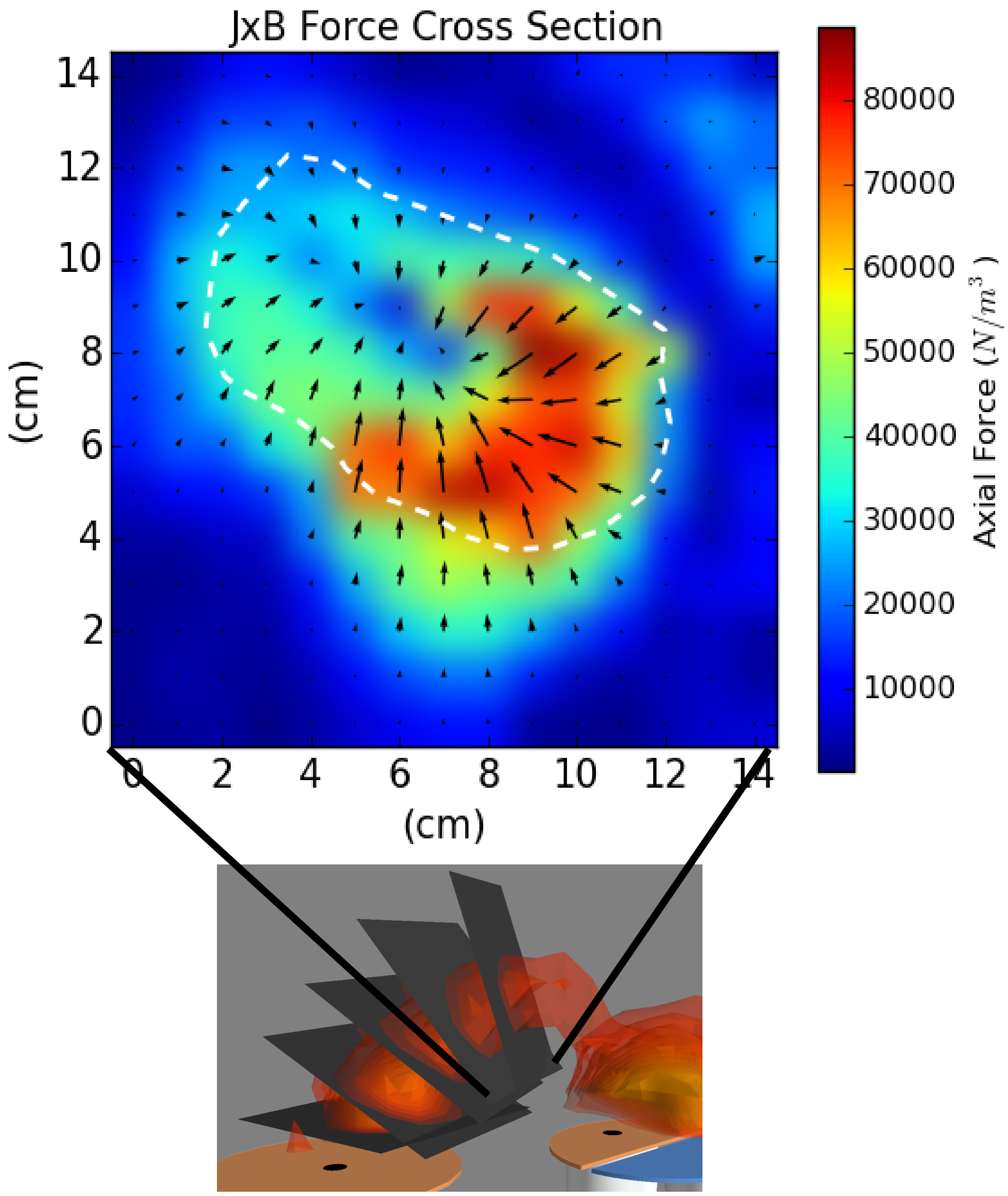

- Out of plane forces shown with colormap
- In-plane forces shown with black vectors
- 50% current radius traced with dotted line

Theory for MHD Axial Force

Any flared current channel (finite J_r) will have an axial JxB force in the direction of larger minor radius

$$(\vec{J} \times \vec{B}) \cdot \hat{z} = J_r B_\phi$$

This is equivalent to the component of magnetic pressure in the axial direction:

$$f_{\hat{z}}[N/m^3] \approx \frac{d}{dz}(\frac{B_\phi^2}{\mu_0})$$

Flared current channel

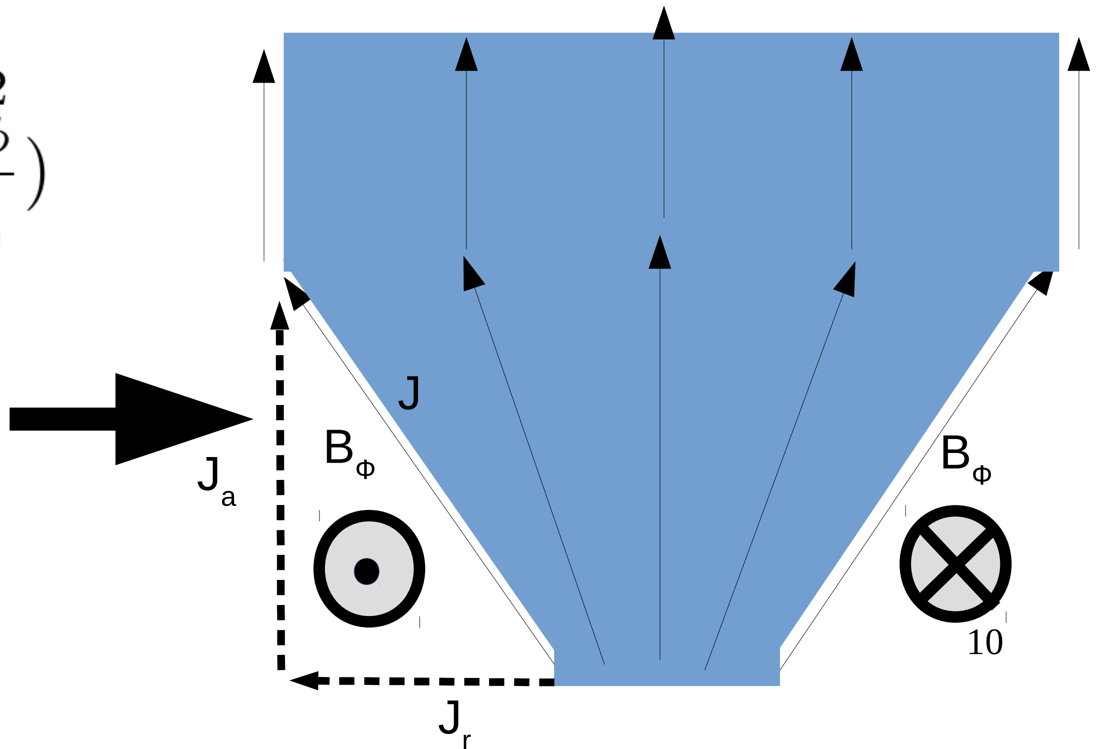

Comparison with Theory

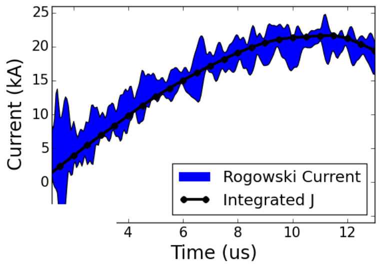

Theory (N/cm)

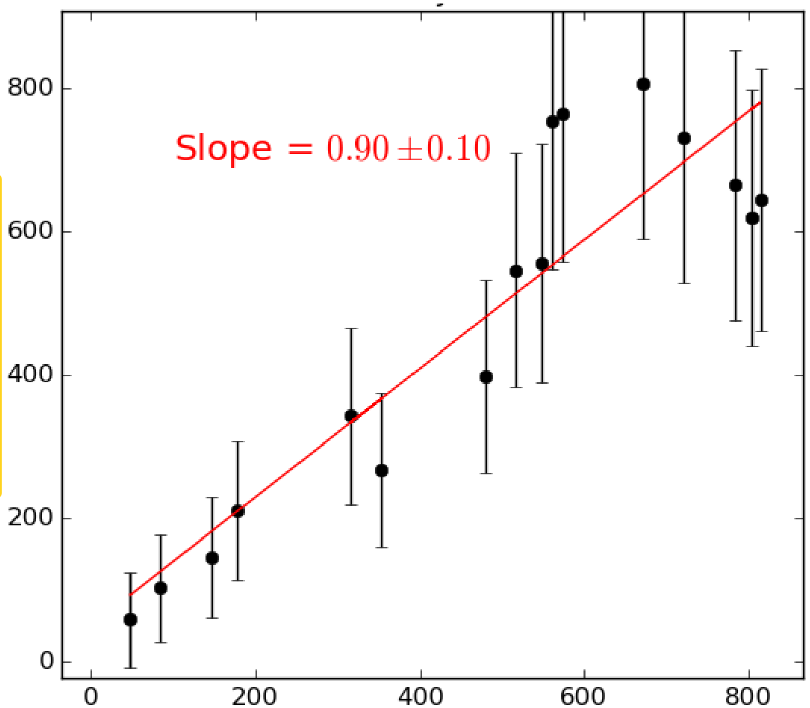

Measured force (N/cm)

Theory predictions calculated from power-supply-current and current channel width, σ(z)

$$\int_A f_{\hat{z}}[N/m^3]\ dA \approx \frac{I^2 \mu_0}{4\pi\sigma} \frac{d\sigma}{dz}$$

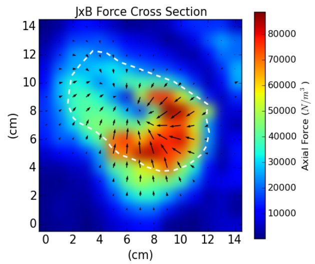

Measurements from integrating out of plane force

Pressure Estimate from Perpendicular Forces

Assuming force balance along the minor radius, we have:

Force balance in minor radius	$P(r) = \int_{\infty}^{r} -\mathbf{J} \times \mathbf{B} \cdot \hat{r} \, \lvert dr' \rvert$

Due to asymmetry of measurement data, we integrate along multiple different rays to bound the on-axis pressure. Rays parallel to hoop force will overestimate pressure, rays anti-parallel to hoop force will underestimate pressure.

Rays taken for pressure integration

Hoop force asymmetry

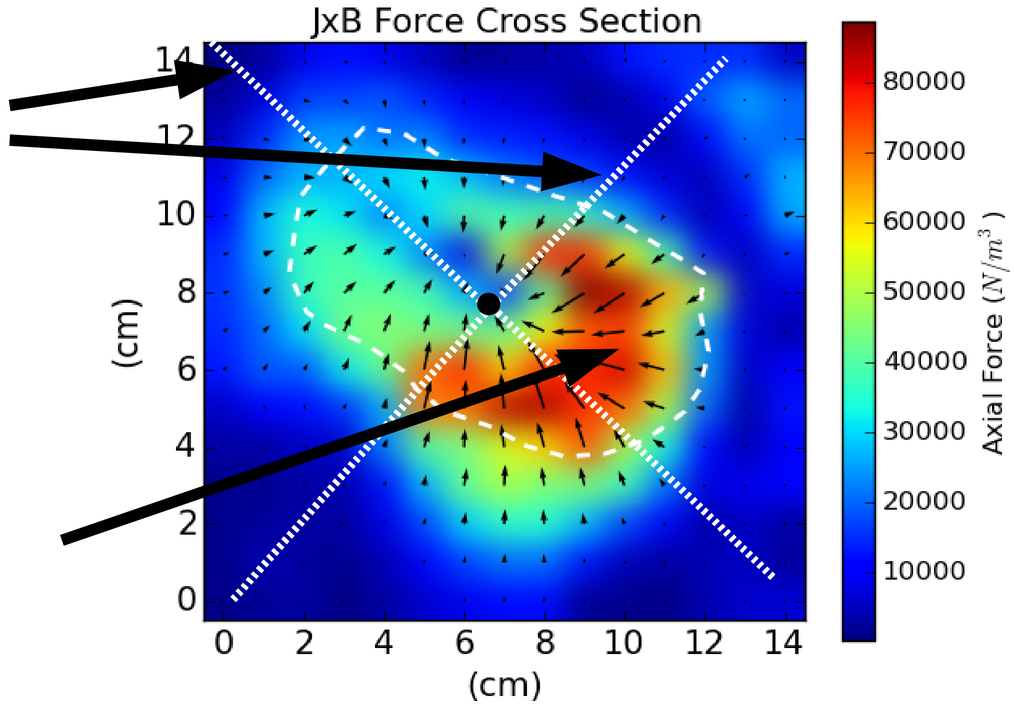

Number Density

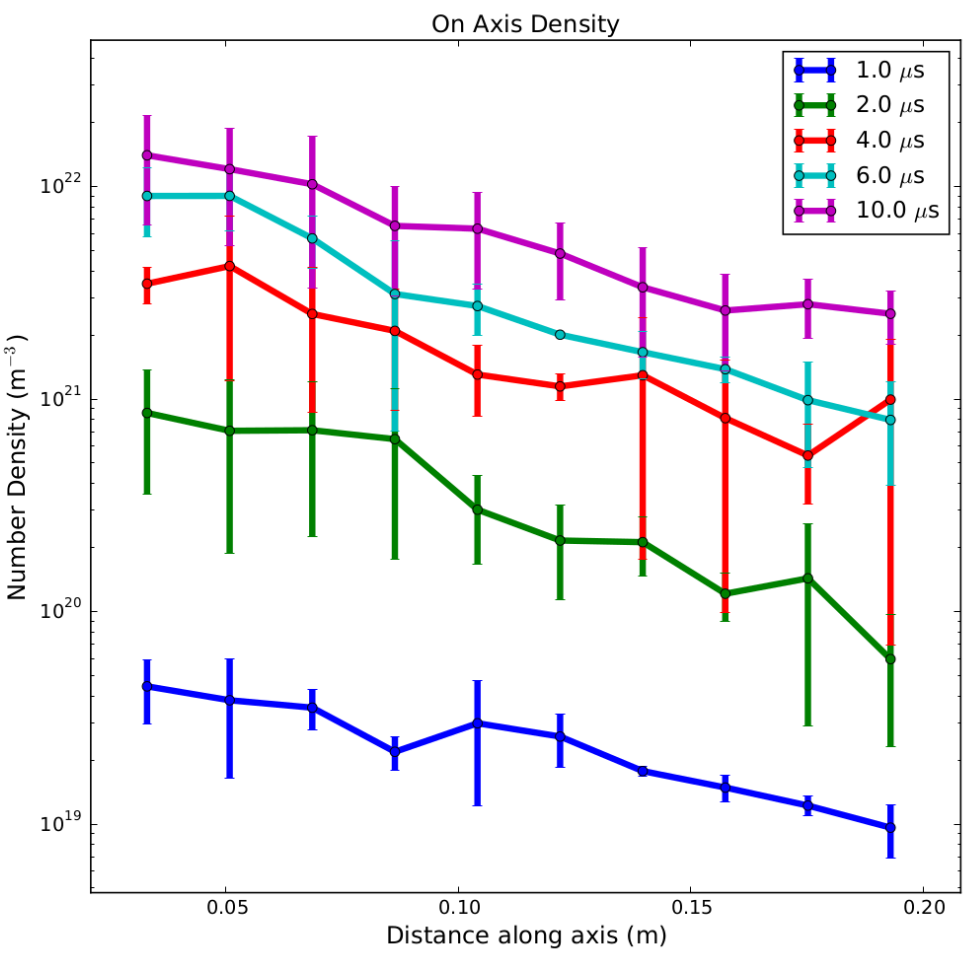

Assuming relatively constant temperature (1-3 eV), we can calculate the number density:

$$\frac{N}{V} = \frac{P}{RT}$$

This gives reasonable bounds on the number density present in the flux tube.

- 300x increase in density
- Background gas cannot account for more than first factor of 10.
- Most density must originate from footpoints

Strong mass flux from boundary!

Inferred Flow Speeds

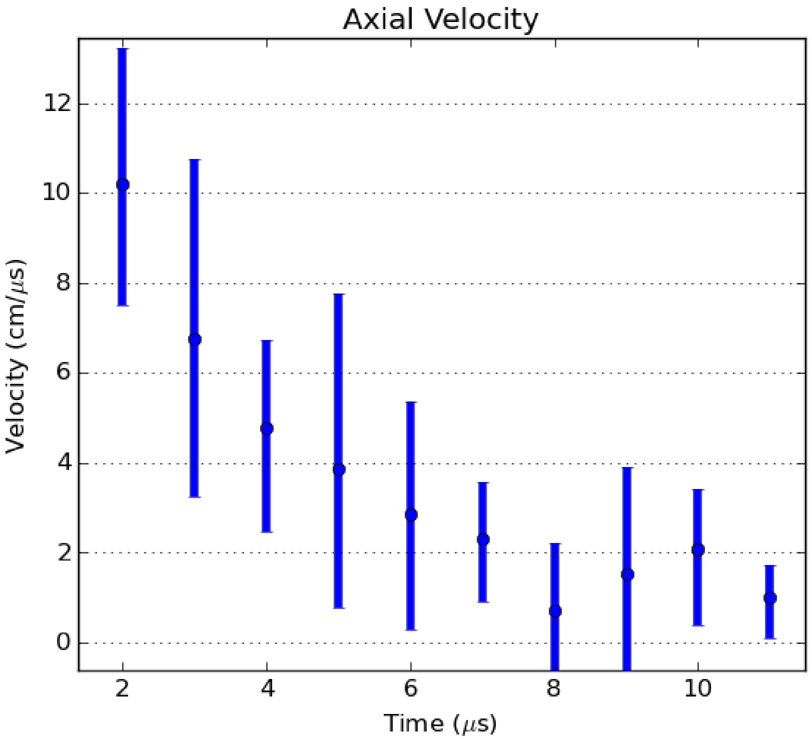

Since we have estimates of density as a function of space and time, we can use the continuity equation to estimate the velocities needed to produce the observed mass flux.

$$\frac{\partial \rho}{\partial t} = -\nabla \cdot (\rho \mathbf{u}) \approx -\left(\frac{\partial \rho}{da} u_a + \frac{\partial u_a}{da} \rho\right)$$

Assuming the compressible term is small near the electrodes:

$$u_0 \approx -\left.\left(\frac{\partial \rho}{\partial t}\left(\frac{\partial \rho}{da}\right)^{-1}\right)\right|_{a=0}$$

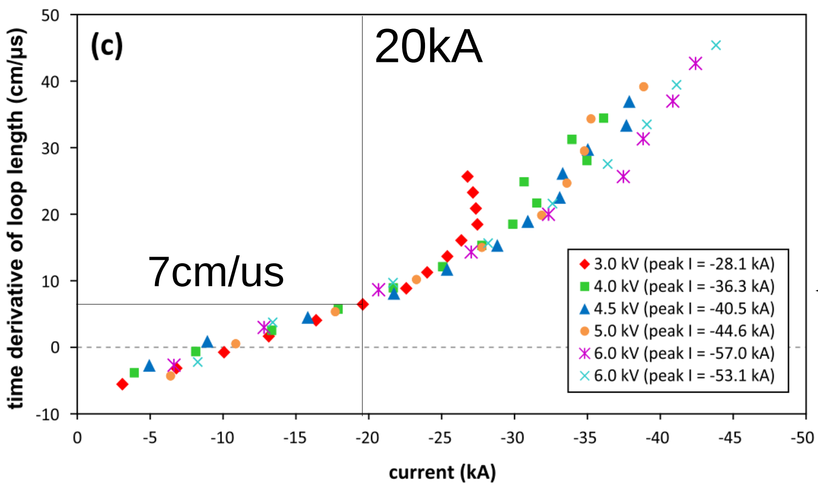

Axial flows observed in similar solar experiment for same currents have the same magnitude (~ 5 cm/us).

Stenson, Eve Virginia, and P. M. Bellan. "Magnetically driven flows in arched plasma structures." PRL 109.7 (2012): 075001.

Axial Forces Consistent with Observed Flows

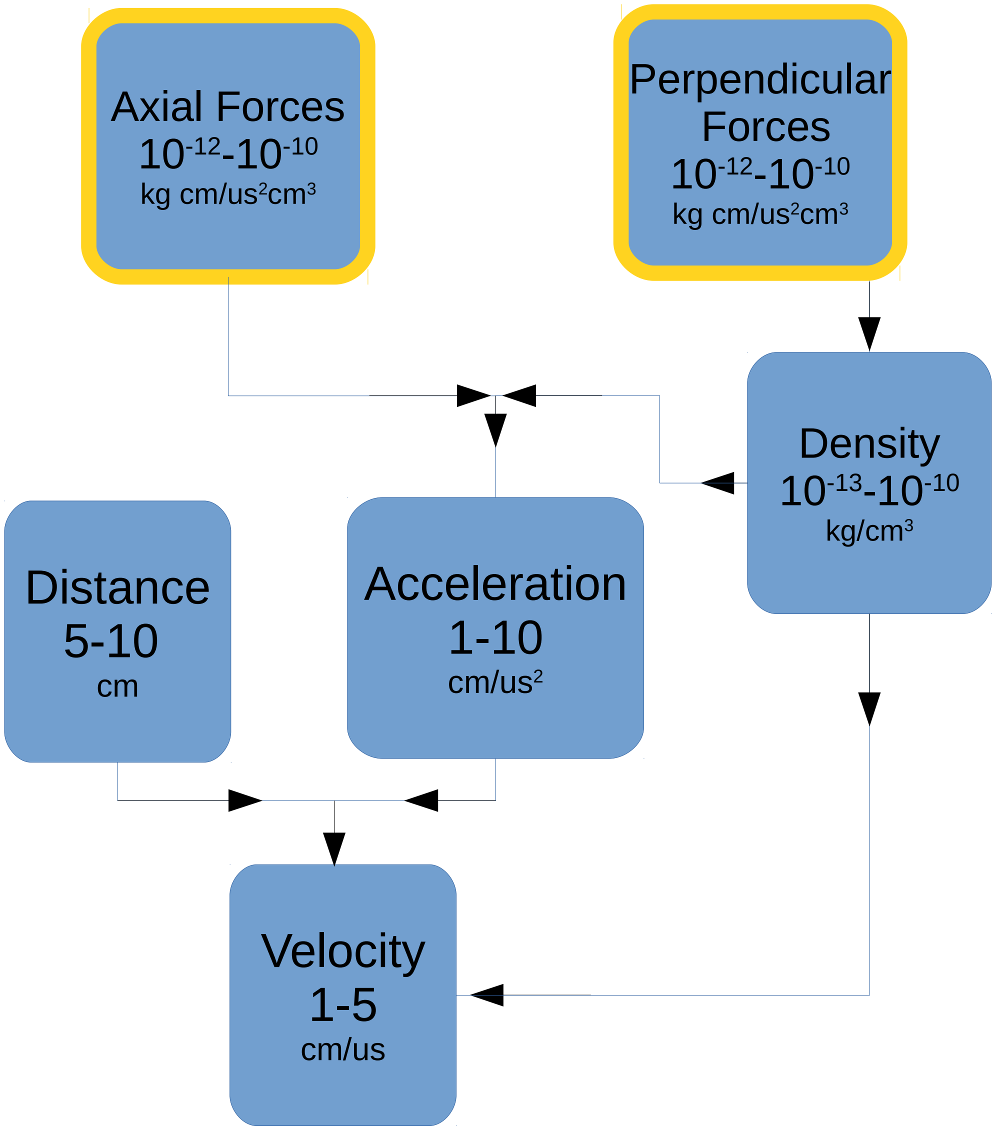

- Measurements of axial and perpendicular forces give two self-consistent estimates of axial velocity
- Inferred velocity from imaging gives same order of magnitude

- Alfvenic axial flows can be driven by axial MHD forces

Axial Field Collimation

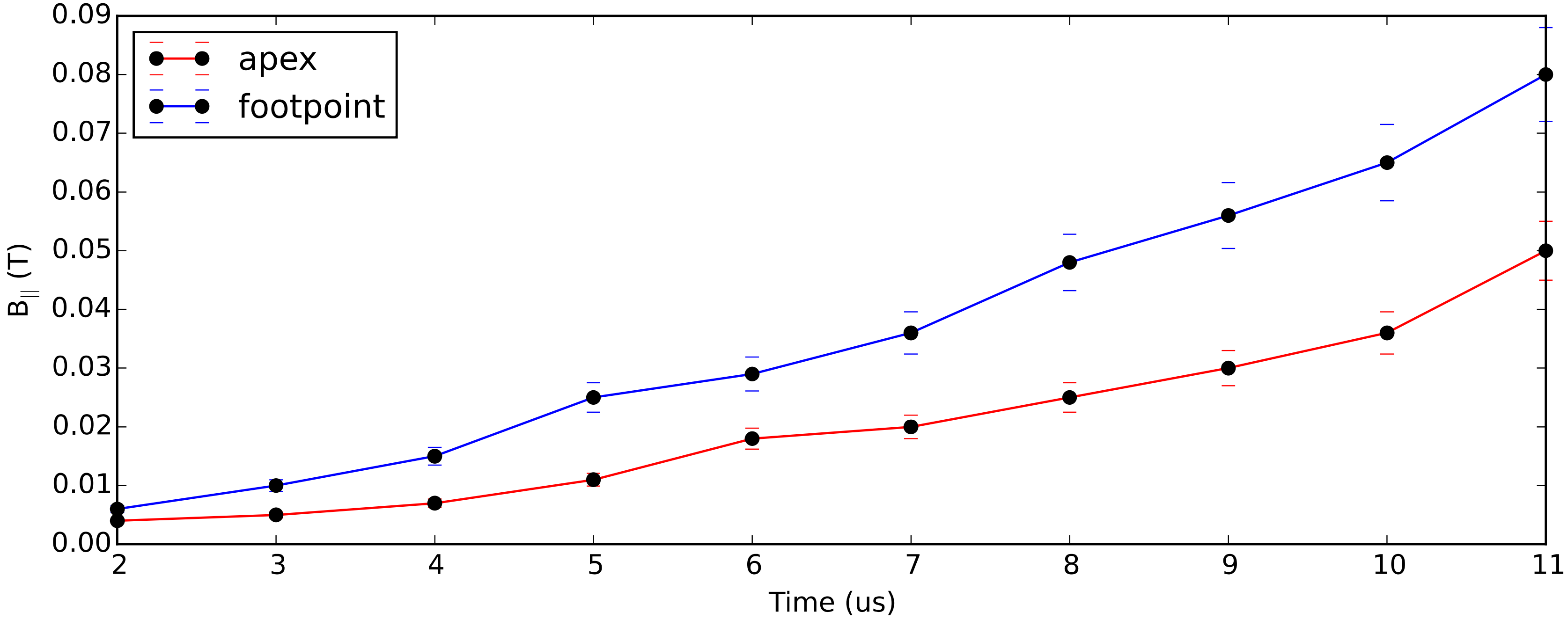

- Axial field increases by factor of 10 during lifetime
- Factor of 3 radial compression (self-similar)

Summary

(1) Laboratory plasma experiment (20 kA, 3kV, 10us, 1m)

(2) 3D MHD force measurements demonstrate simple self-consistent mechanism for mass flux from flared current channel.

(3) Mass flux relevant to dynamics of coronal loops, astrophysical jets, and compact tori.

Relaxation as a dynamic cascade

Double Coronal Loop Experiment

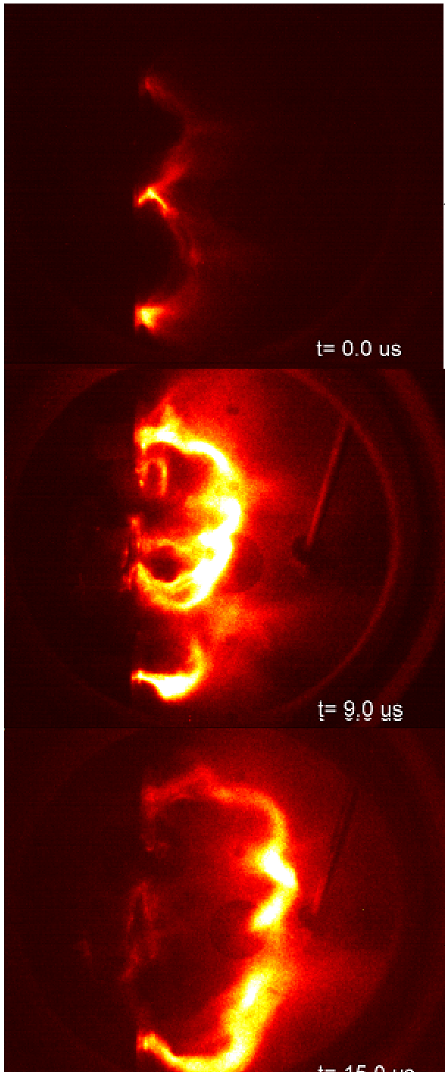

Helicity Injection

Nontrivial
Boundary Conditions

Sheath Effects

Flows and Collimation

Finite beta

Non-equilibrium
evolution

Kink and Secondary Instabilities

Hall Reconnection
Wave coupling
Nonthermal heating

Astrophysical Jet Experiment

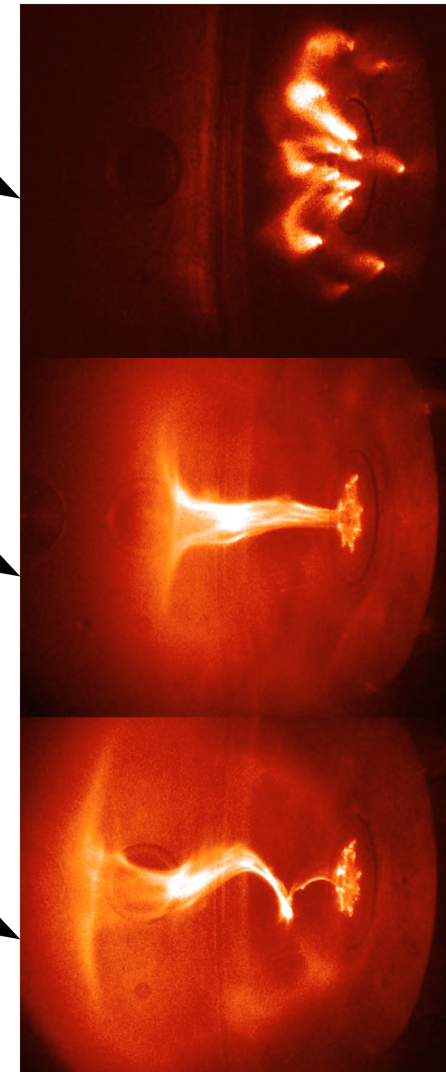

Formation of plasma jet

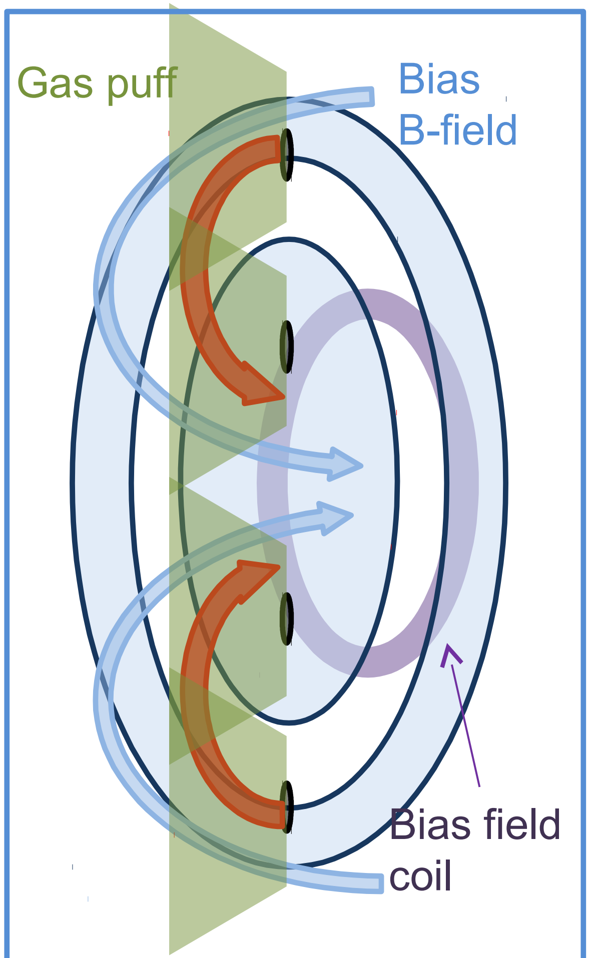

8 plasma-filled flux tubes form along the bias field

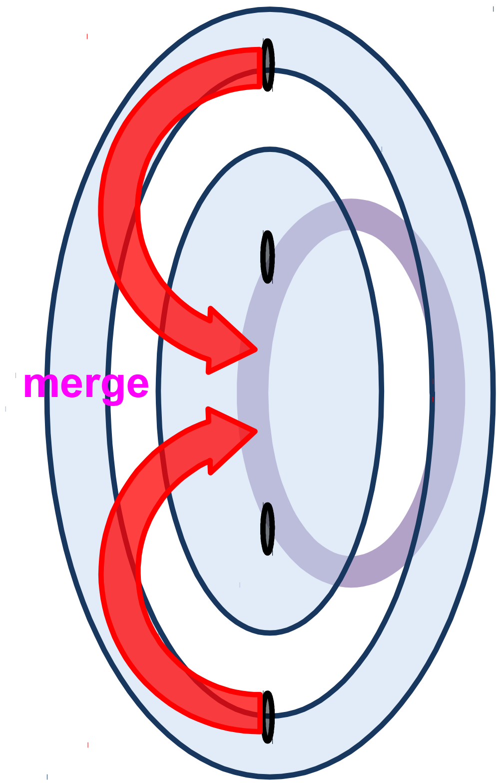

Currents in the same direction attract each other, jet forms

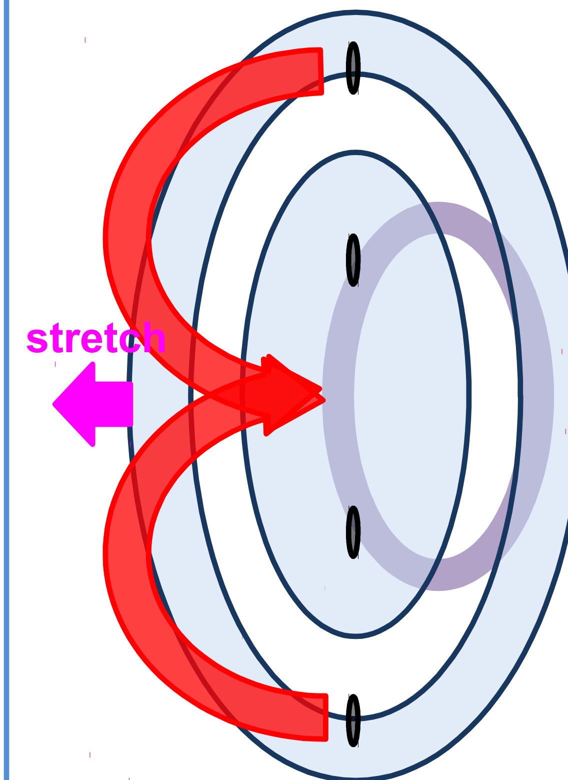

Axial gradient of **JxB** force, jet stretches

Ideal MHD kink instability

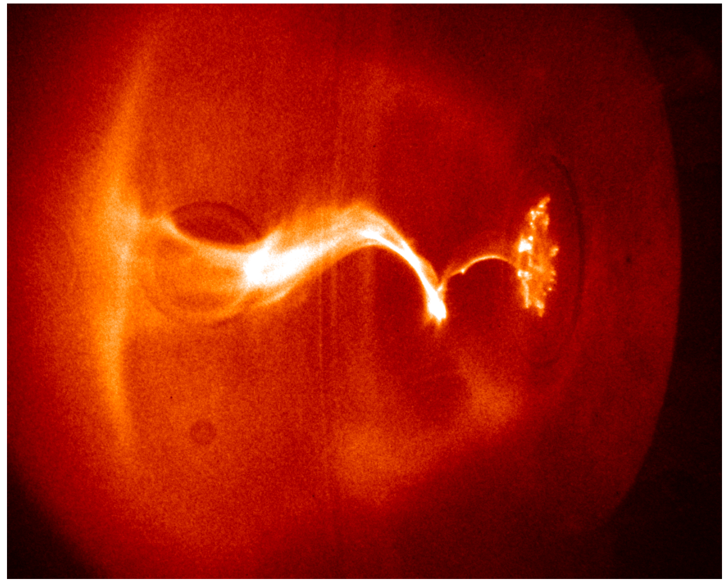

- As jet length exceeds a critical value plasma becomes kink unstable
- Can be explained by Kruskal-Shafranov criterion:
  - $q = rB_z/RB_\phi = 2\pi rB_z / LB_\phi$
  - L increases → q decreases: kink occurs when $q < 1$

S. C. Hsu and P. M. Bellan, PRL **90**, 215002 (2003).

Rayleigh-Taylor (RT) instability

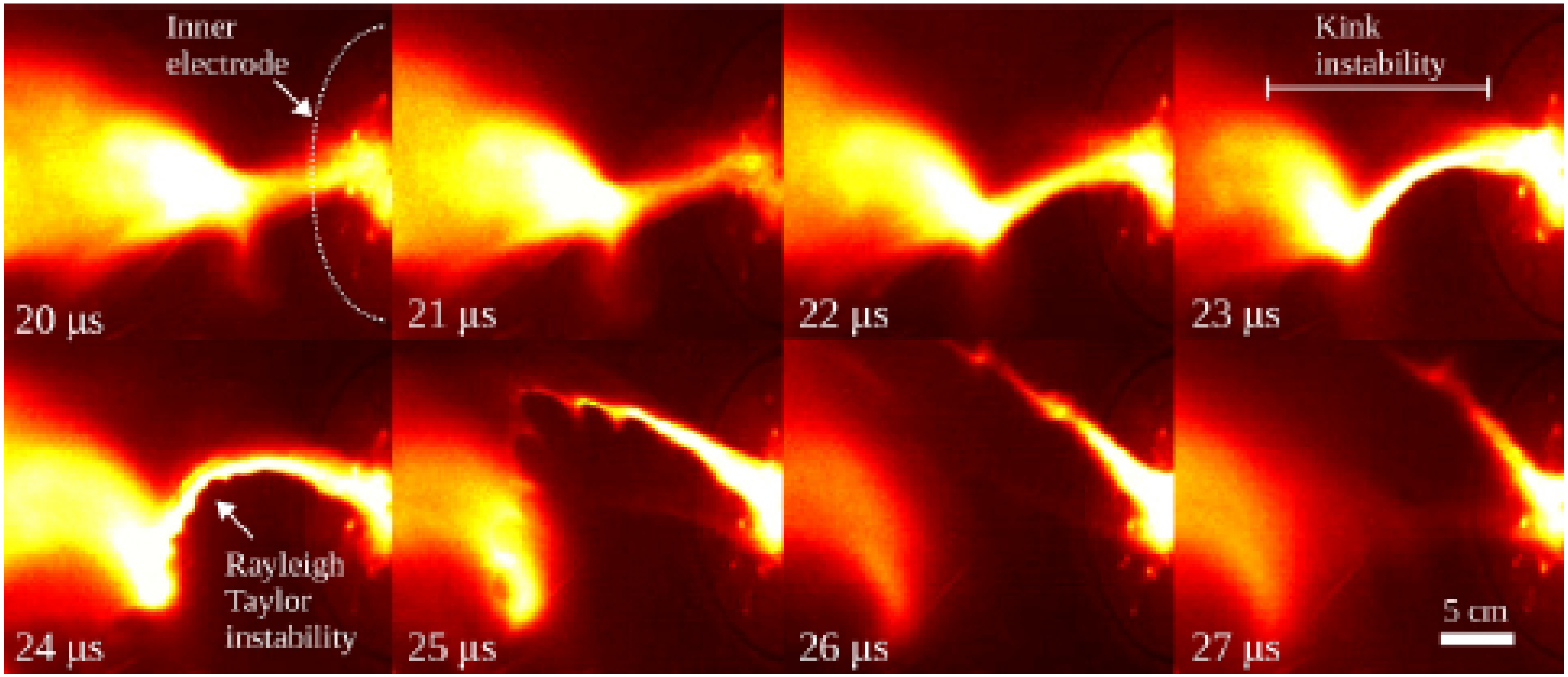

- Kink instability induces effective gravity in the – r direction
- RT instability occurs at interface between heavy plasma and light vacuum
- Finger-like structures: RT ripples.

A. L. Moser and P. M. Bellan, Nature **482**, 379 (2012).

Kink-induced Rayleigh-Taylor (RT)

- **Kink-induced Rayleigh-Taylor instability severs plasma jet.**
- We **simultaneously observe:**

1) Strong, localized 25-40 nm EUV bursts
2) Doppler and Stark broadenings in plasma emission spectra
3) 2-20 MHz polarized B-field fluctuations
4) Strong and transient voltage spikes
5) Sudden changes in B-field profile

❑ **Conclusion**: Hall-MHD magnetic reconnection occurs and causes Ohmic electron heating, stochastic ion heating, whistler wave emission

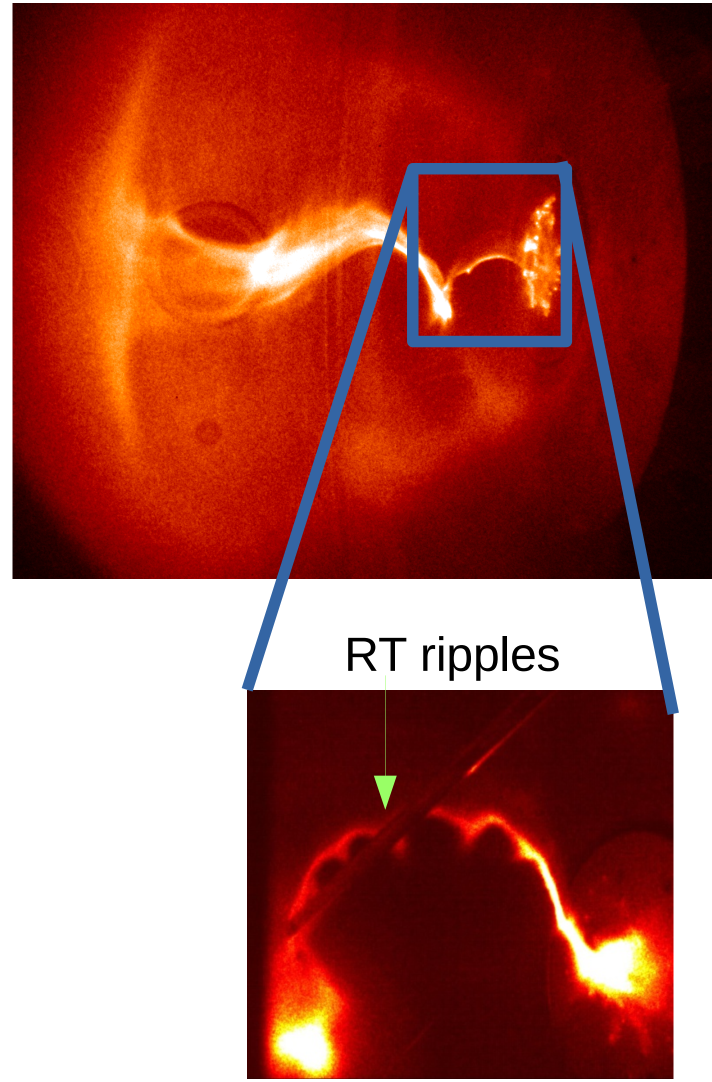

Not the same shot

K.-B. Chai, X. Zhai, P. Bellan, Phys. Plasmas **23**, 132122 (2016).

Diagnostics for investigating RT signatures

High frequency B-dot probe measures whistler waves

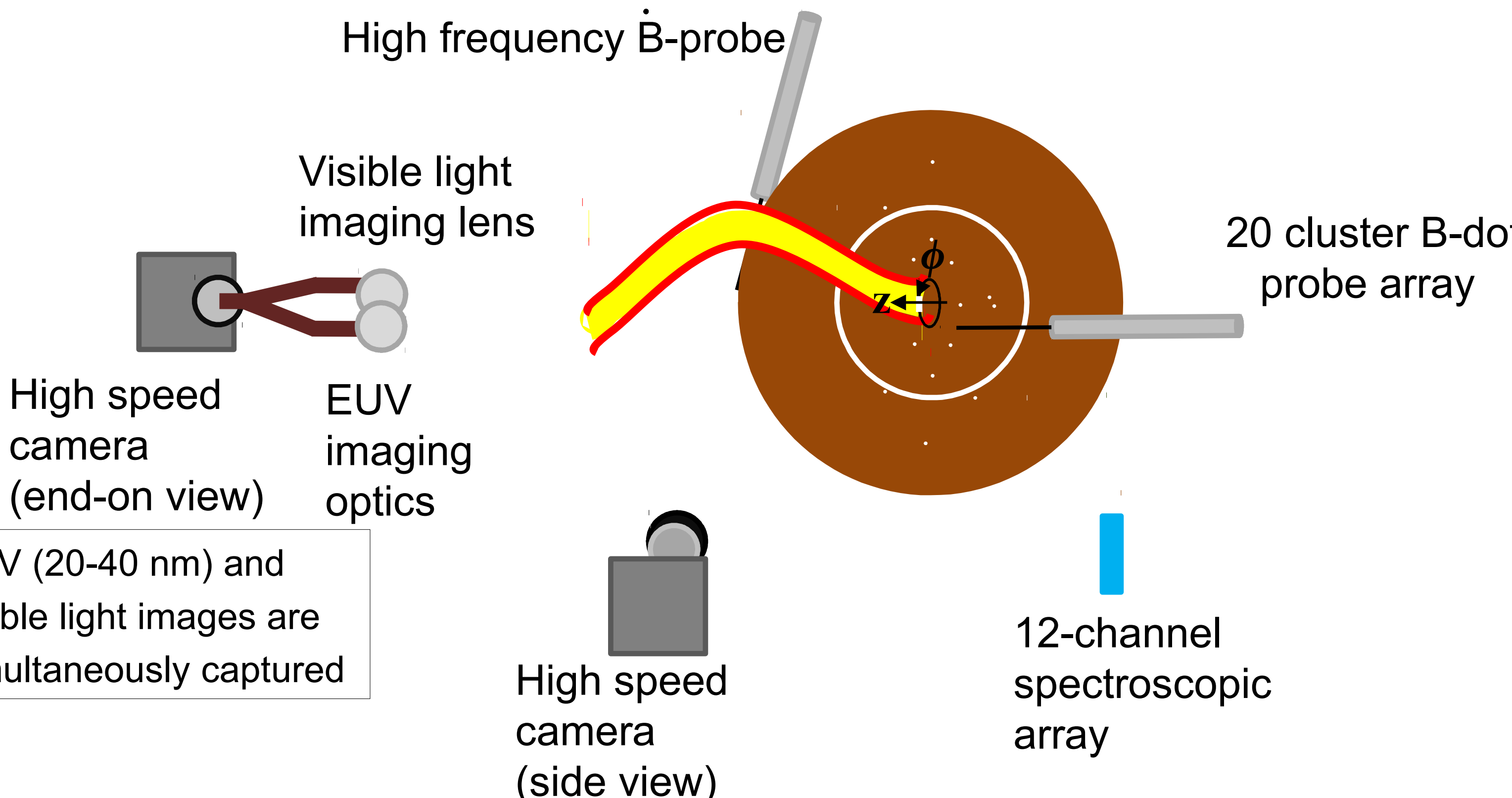

EUV (20-40 nm) and visible light images are simultaneously captured

Spectroscopic system measures Doppler and Stark broadenings

Simultaneous EUV and RF bursts

- Observe transient EUV bursts & high frequency fluctuations when RT occurs:
  - EUV bursts: could be associated with electron heating
  - High frequency fluctuation: could be associated with whistler waves
- Goal: study details of magnetic reconnection occurring in our jet by using comprehensive diagnostics

Filtered PIN diode signal

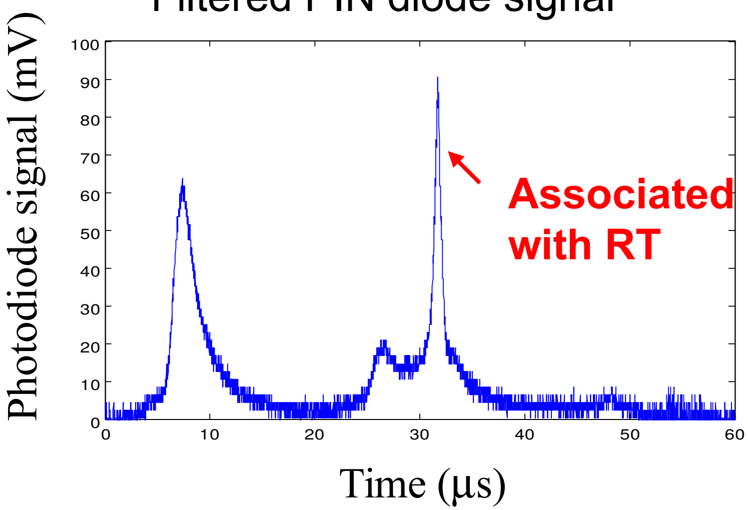

K.-B. Chai & P. Bellan, Rev. Sci. Instrum. **84**, 123504 (2013)

Capacitively-coupled probe signal

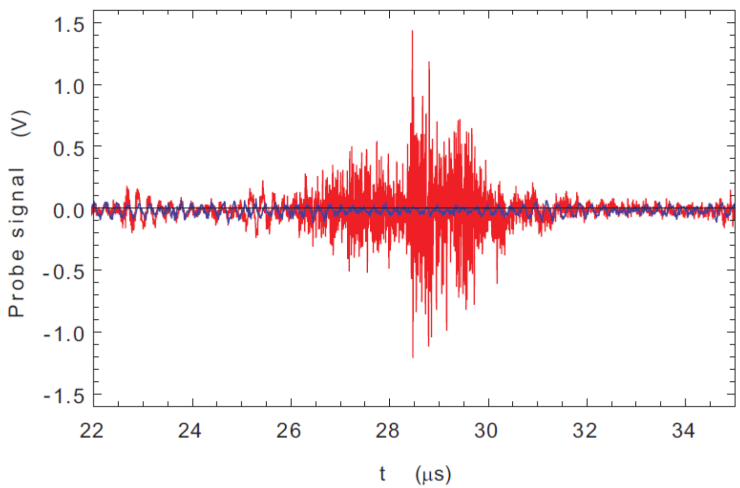

A. L. Moser & P. Bellan, Nature **482**, 379 (2012)

EUV imaging optics

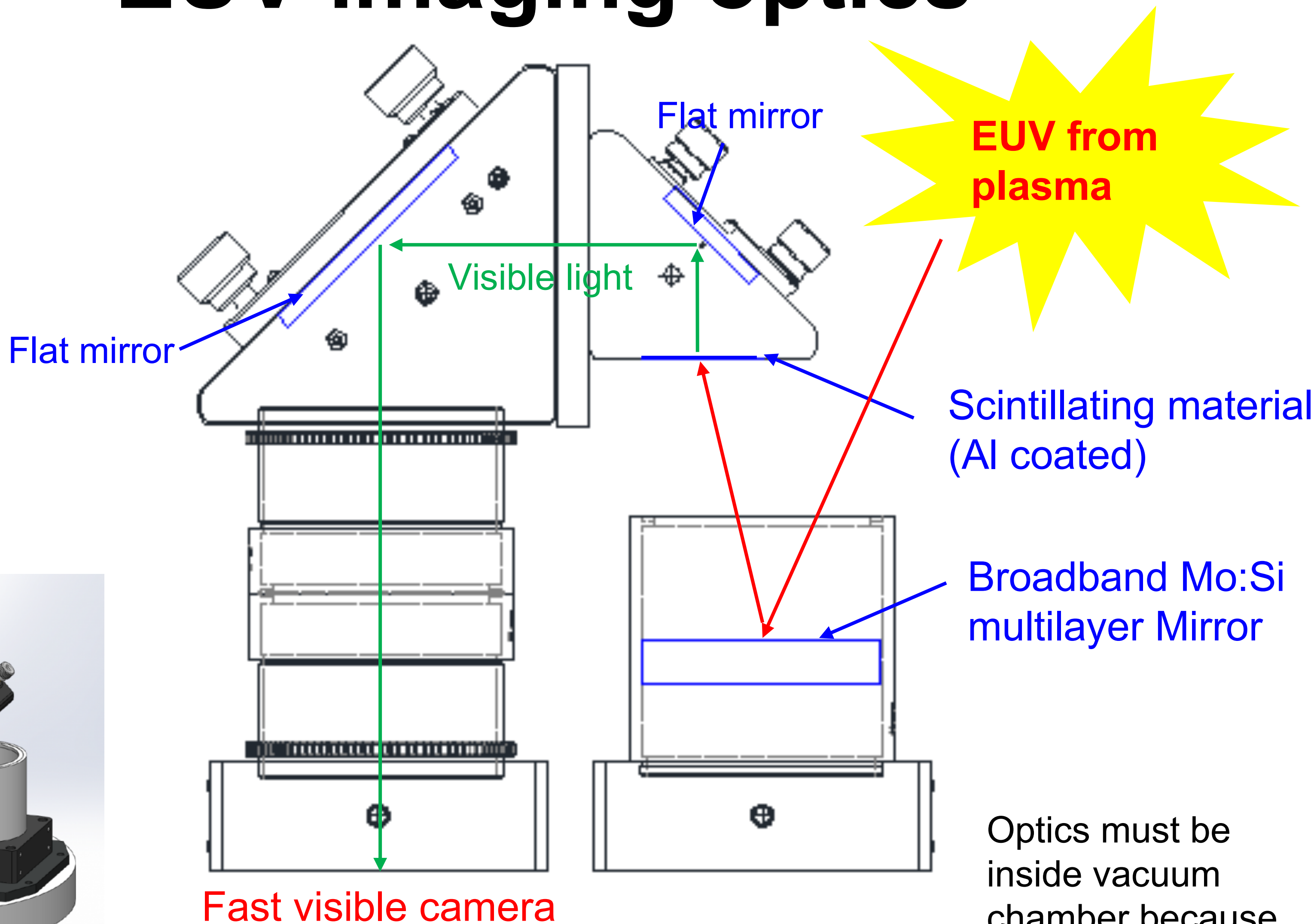

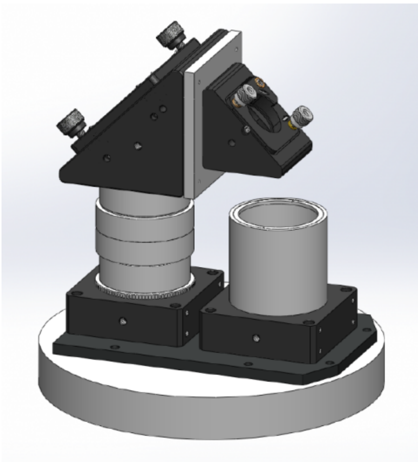

Optics must be inside vacuum chamber because EUV cannot pass glass window

K.-B. Chai and P. M. Bellan, Rev. Sci. Instrum. **84**, 123504 (2013).

EUV (25-40 nm) vs visible light

End-on view

red: EUV; blue: visible light

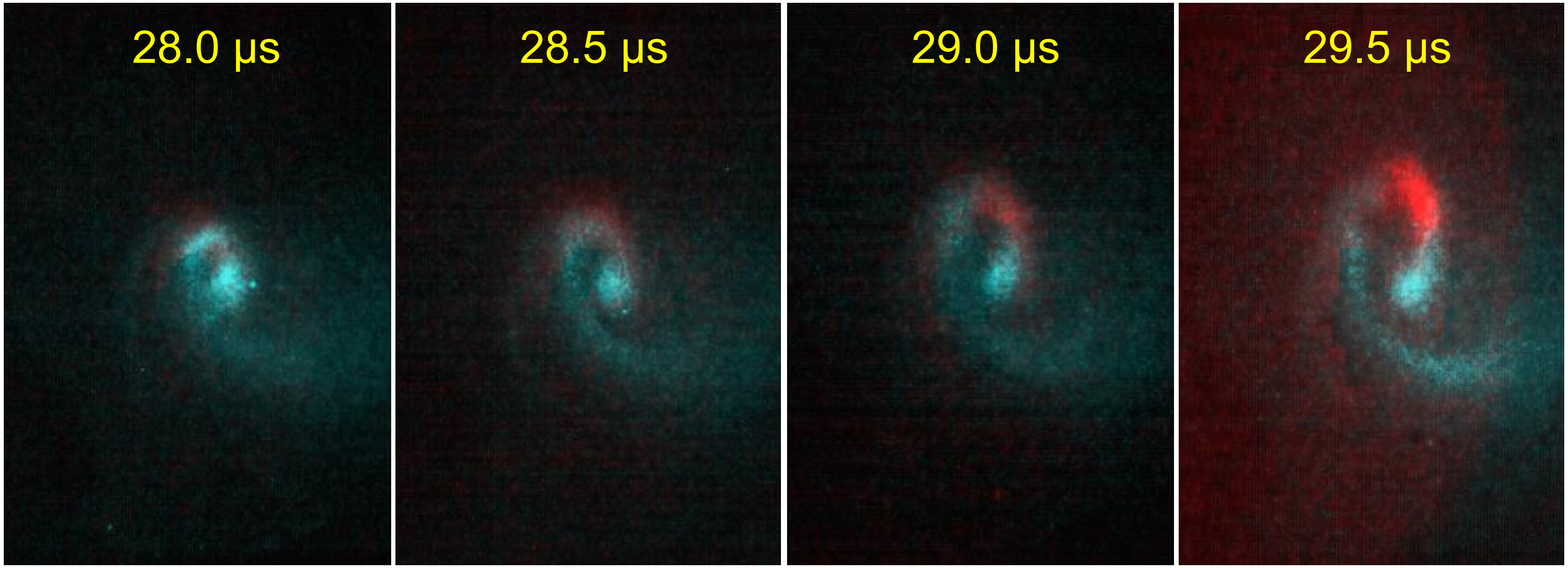

- As RT instability grows:
  - EUV (red) becomes extremely bright in localized area
  - Visible light (blue) becomes dark where EUV gets bright

→ Ratio of EUV to visible light becomes extremely high

→ Higher ionization state when RT occurs (electron heating)

Electron heating: Spectroscopic line ratios

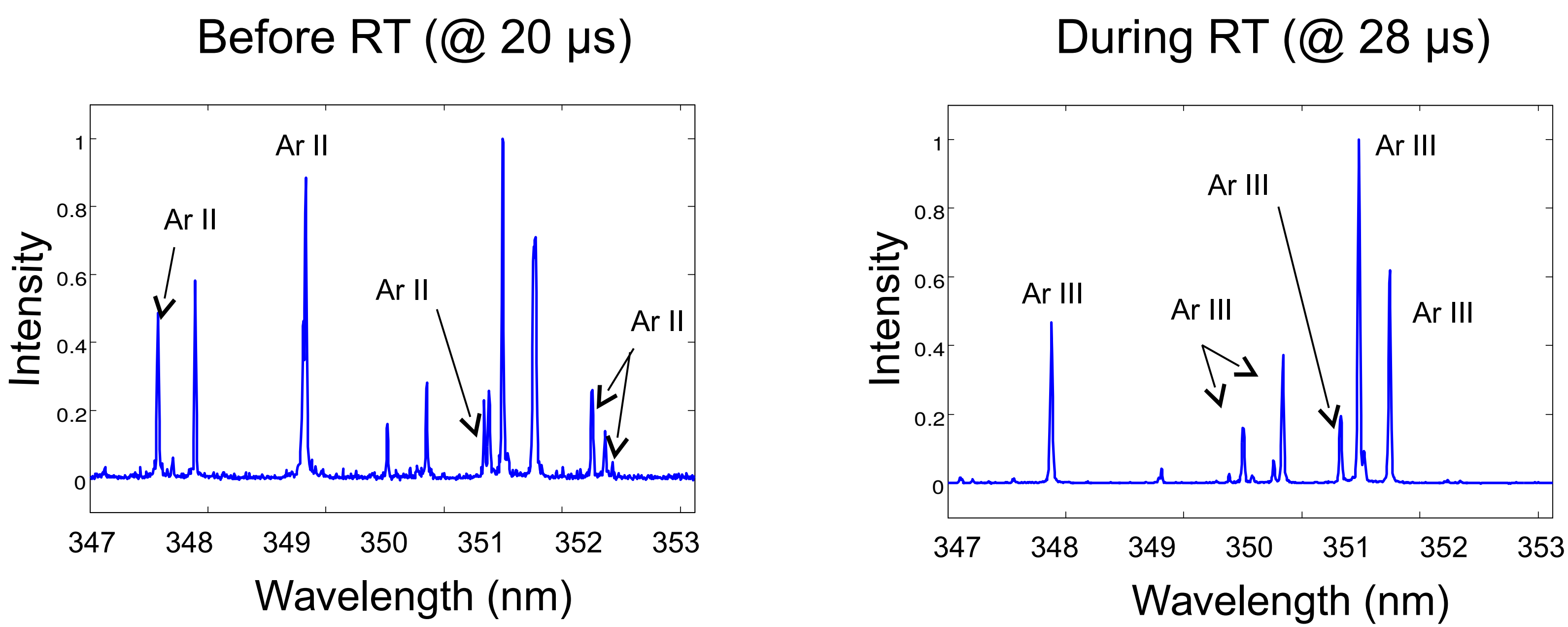

- As RT occurs:
  - Ar II (Ar^+) lines disappear and Ar III (Ar^{2+}) lines dominate over Ar II lines
  - Ar IV (Ar^{3+}) lines are also observed

→ Indicates higher ionization state and electron heating

Ion heating: Doppler & Stark broadening

Before RT (@ 20 μs)

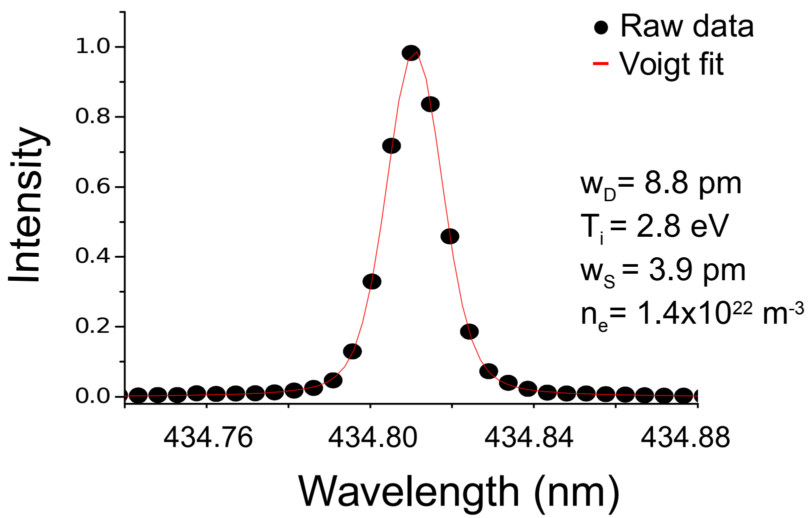

During RT (@ 28 μs)

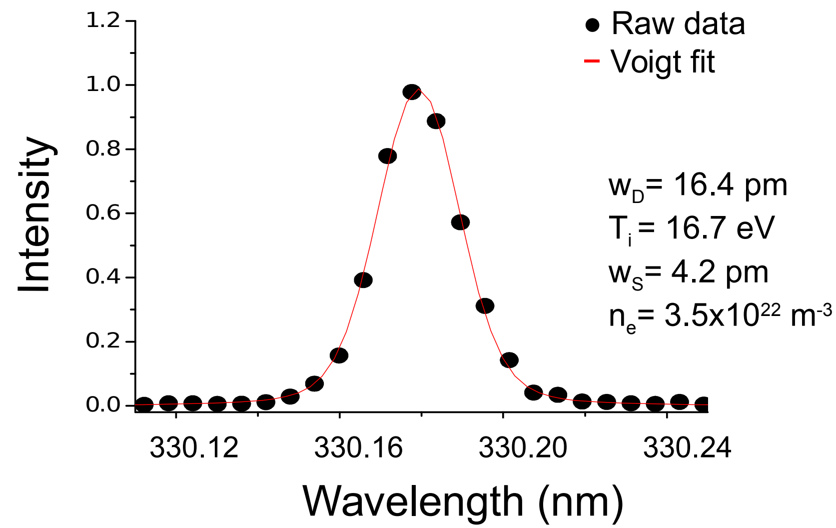

- Voigt fitting gives both Doppler (T_i) and Stark (n_e) broadenings:
- As RT occurs
  - T_i: 2.6 ± 0.4 eV - 15.8 ± 2.3 eV
  - n_e: $(1.6 \pm 0.3)\times10^{22}$ m^{-3} - $(5.1 \pm 2.1)\times10^{22}$ m^{-3}

High frequency B-dot probe

- B-dot probe with excellent shield

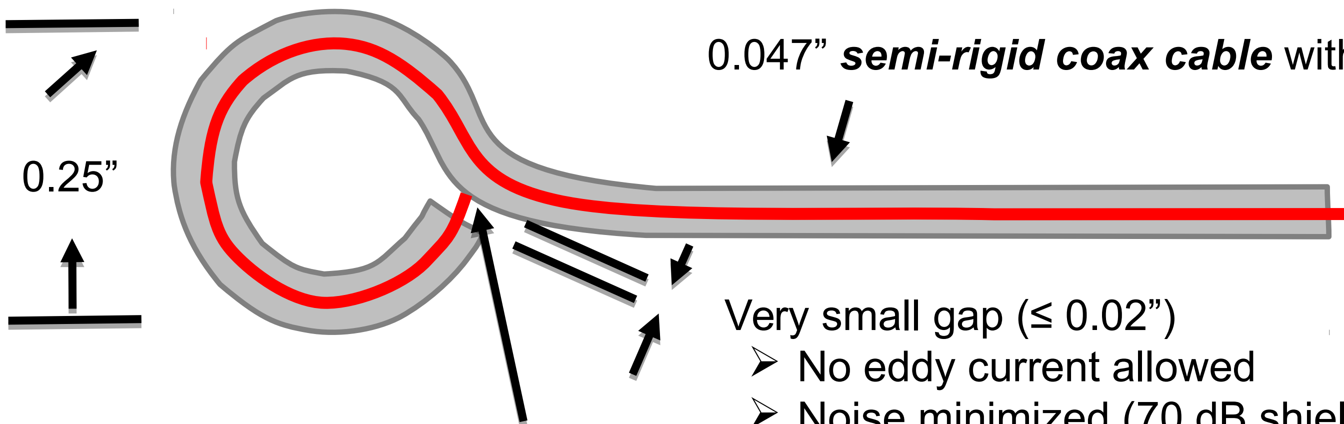

- Equivalent circuit

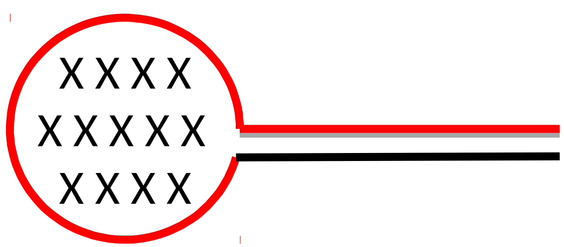

$$V_{out} = \frac{d\Phi}{dt} = A\frac{dB}{dt}$$

Whistler waves: Magnetic field fluctuations

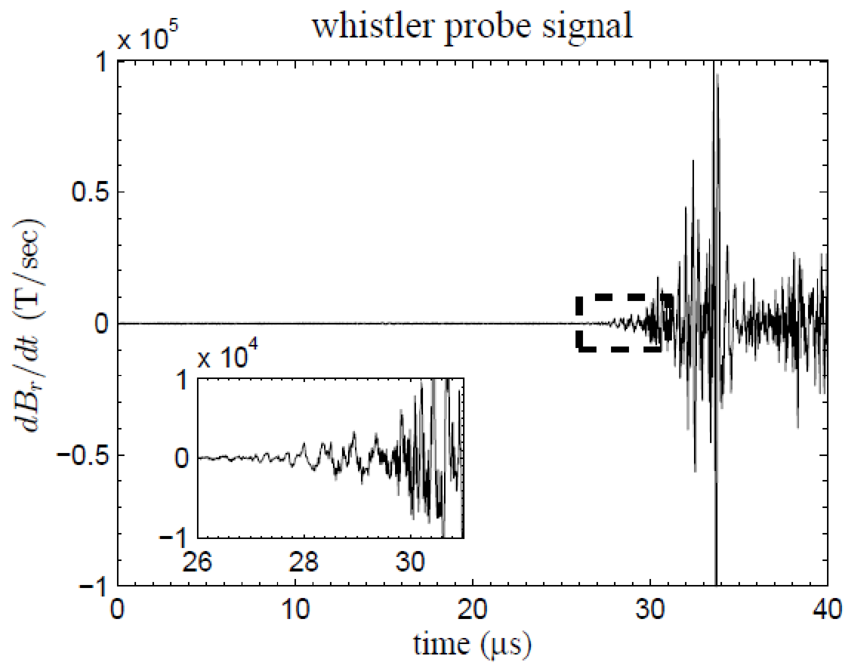

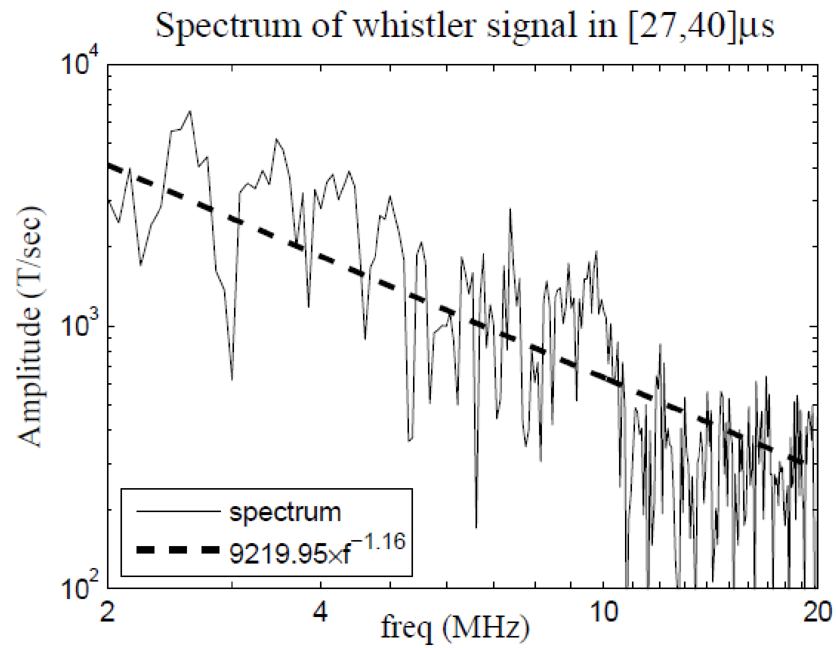

- As RT occurs, broadband (2-20 MHz) high frequency magnetic fluctuations measured by whistler probe.
  - Ion cyclotron freq. < observed wave freq. < electron cyclotron freq.
  - Have power-law dependence on freq. (~ f^{-1}) but not turbulence because of coherence between different frequencies

Whistler waves: Circular polarization

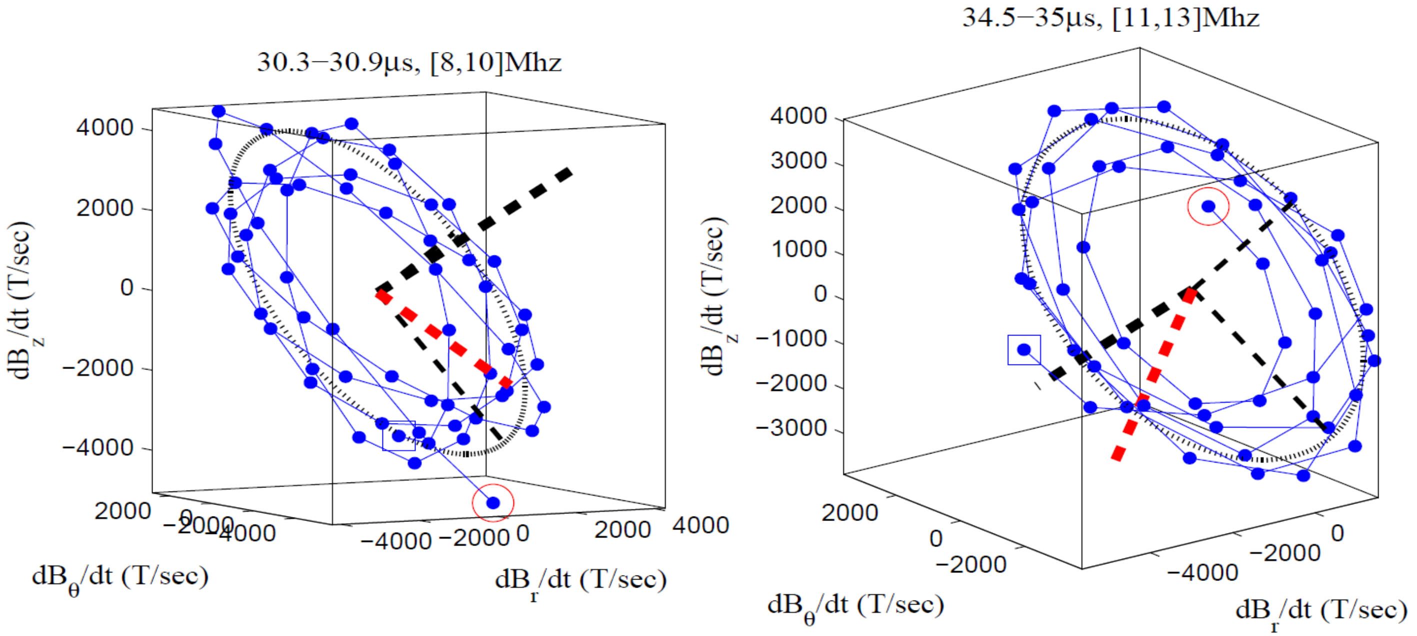

- Hodograms of magnetic vector show circular polarization: confirms whistler wave character
  - Angle between waves and background magnetic field: < 60°
- **<u>Observation of whistler waves suggests Hall-MHD reconnection</u>**

Voltage spikes

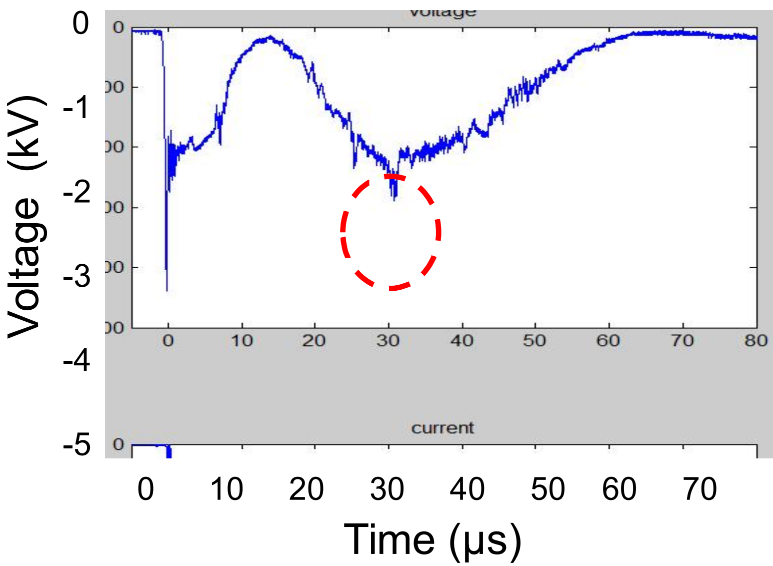

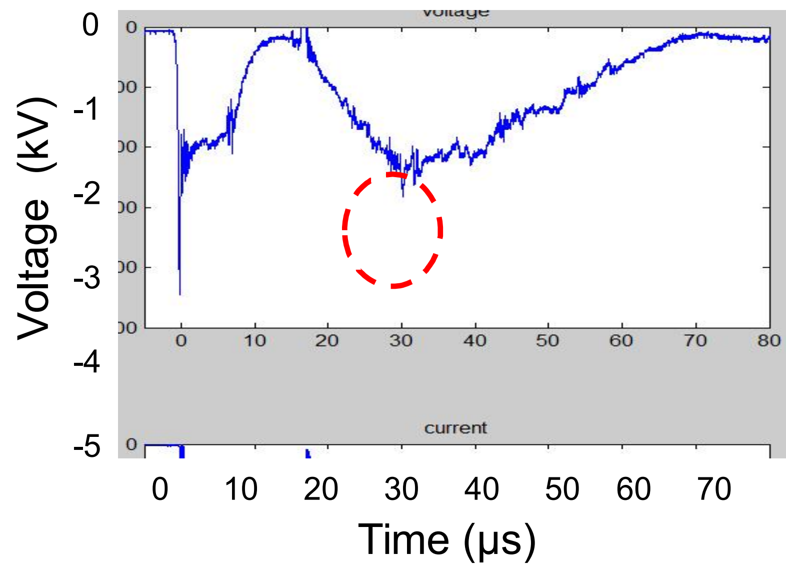

- When RT breaks the jet:
  - Reproducible, >500 V voltage spikes lasting ~1 µs appear
- Interpretation: sudden break of jet current induces strong emf

Conclusion

- Hall-MHD reconnection is believed to occur because

  1) jet diameter is observed to be similar to ion skin depth

  2) whistler waves are observed

  3) Hall term and resistive term are calculated to have same order of magnitude
- Electron heating is likely caused by Ohmic dissipation
- Ion heating plausibly results from stochastic heating
- Voltage spikes are likely caused by sudden change in magnetic flux linking the electrode circuit

Relaxation as a dynamic cascade

Double Coronal Loop Experiment

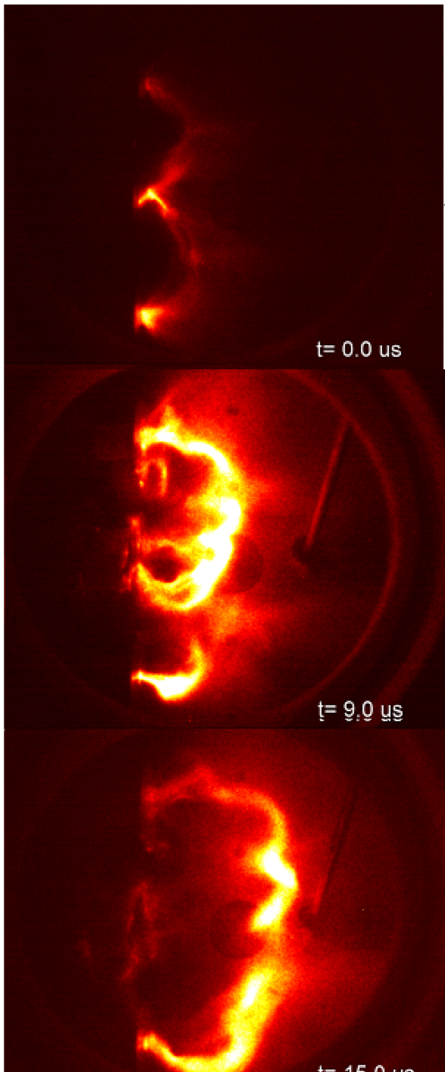

Helicity Injection

Nontrivial
Boundary Conditions

mass flux, B-field, E-field

Flows and Collimation

Finite beta

Non-equilibrium
evolution

Kink and Secondary Instabilities

Hall Reconnection
Wave coupling
Nonthermal heating

Astrophysical Jet Experiment

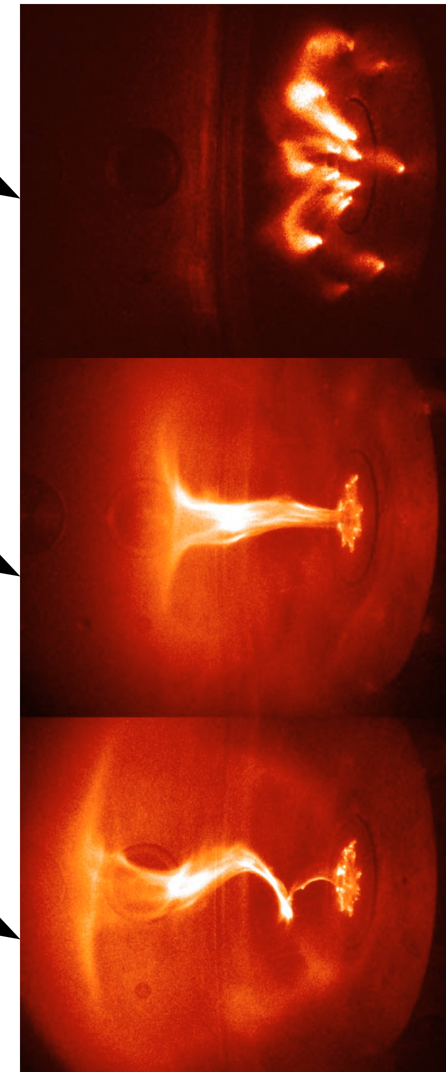

Questions?

Experimental Parameters

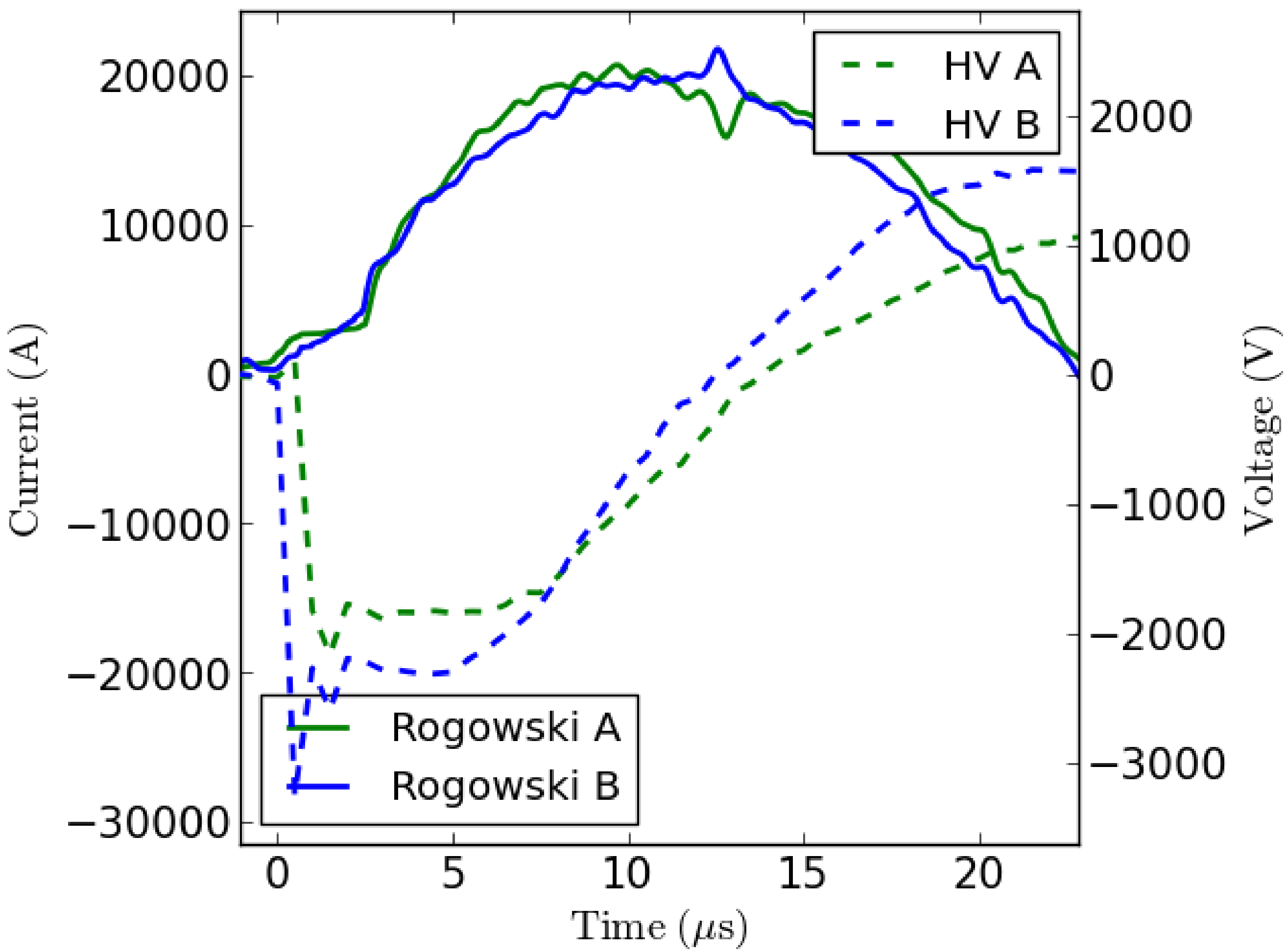

I ~ 20 kA

V ~ 3 kV

L ~ 1 m

dT ~ 10 us

B ~ 0.1 T

n ~ 1e21 m^{-3}

V_A ~ 1e4 m/s

Scintillating material: YAG:Ce Crystal vs powder

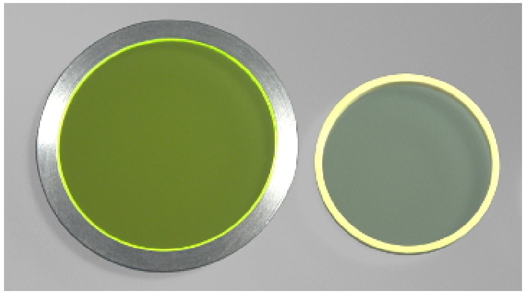

crystal

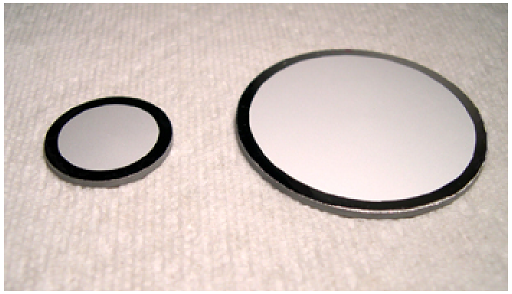

powder

	Crystal	powder
Output wavelength	550 nm	
Decay time	70 ns	
Thickness	100 µm	15 µm
Al coating thickness	200 nm	50 nm
Converting efficiency	1	3
X-ray resistance	strong	weak

→ Powder type has better efficiency because it is thin

Mo:Si multilayer mirror

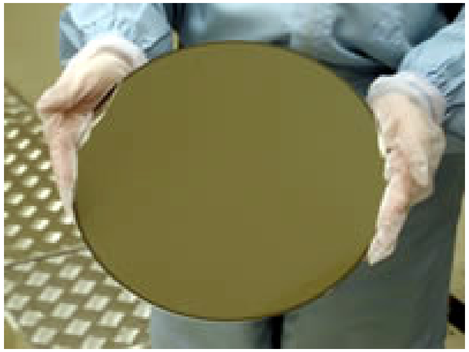

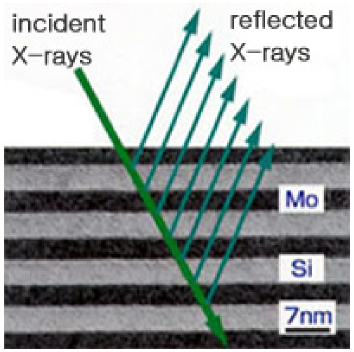

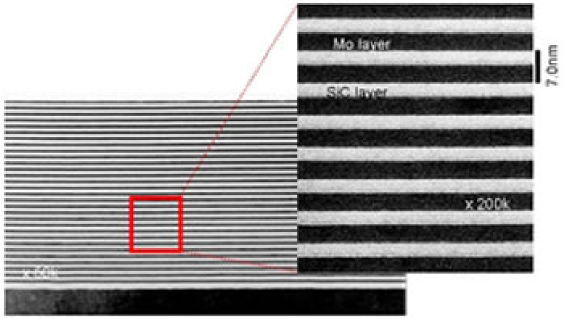

- Forms EUV image onto scintillator
  - Concave shape with f=50 mm; diameter 50.4 mm
  - Multilayered to obtain high reflectivity for 25-41.3 nm EUV
  - Maximum reflectivity **13%** @ 36.5 nm (34 eV) with normal incident
  - Custom manufactured by NTT-AT (Japan)
- Principal: stack Mo/Si periodically to obtain constructive interference
  - Periodicity: satisfy Bragg constructive interference condition
  - $d \sin\theta = \lambda / 2$ (d: periodicity, θ: angle to mirror surface, λ: wavelength)

Efficiency of EUV optics

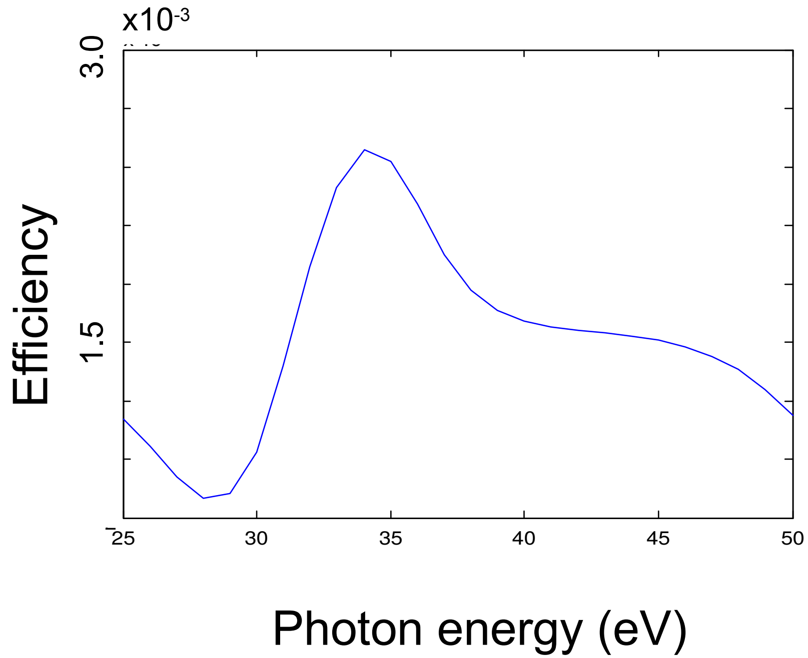

30 eV= 41.3 nm
50 eV= 24.8 nm

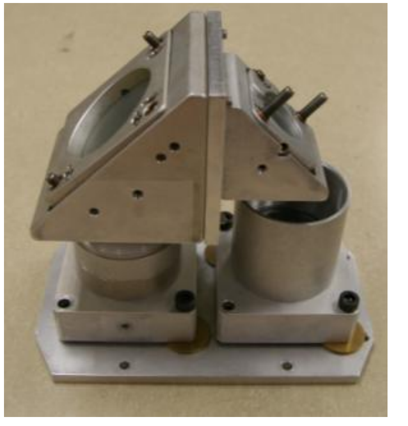

- Efficiency = mirror reflectivity × Al transmittivity × scintillator efficiency
- Maximum efficiency: **~ 0.25 %** @ 36.5 nm (34 eV)
- Average efficiency for 24.8-41.3 nm (30-50 eV) EUV: **0.15 %**

→ **Efficiency looks low but enough for us because our plasma is bright**

High frequency B-dot probe

- B-dot probe with excellent shield

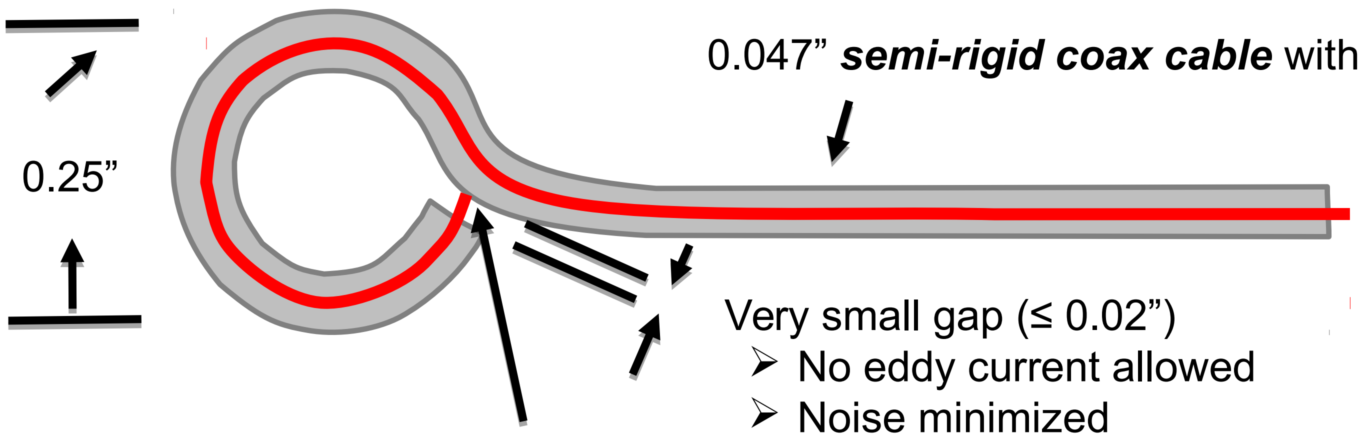

- Equivalent circuit

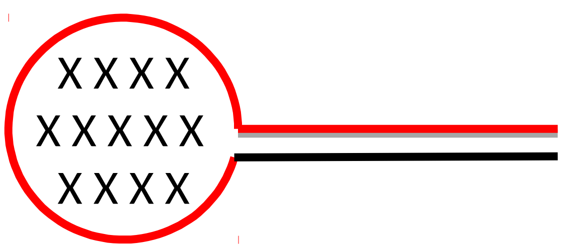

$$V_{out} = \frac{d\Phi}{dt} = A\frac{dB}{dt}$$

Probe pair facing opposite direction

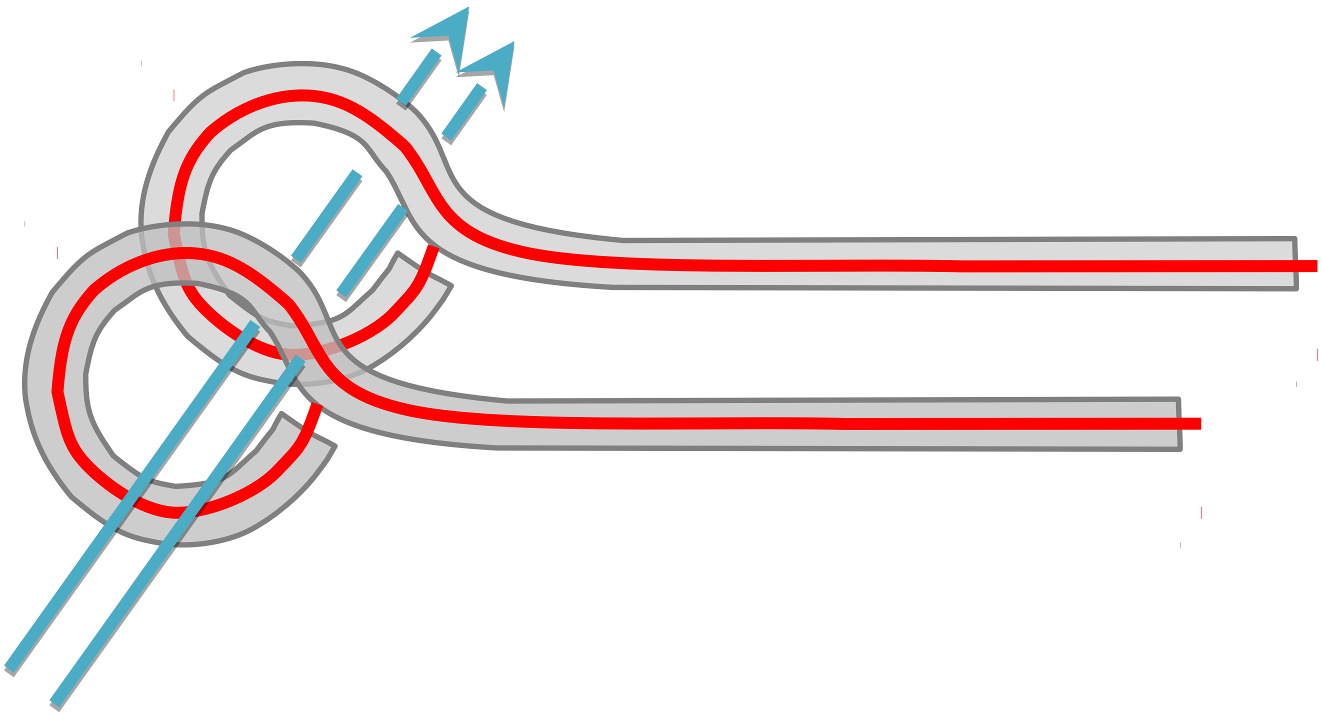

$$V_1 = A\frac{dB}{dt} + V_{common}$$

$$V_2 = -A\frac{dB}{dt} + V_{common}$$

- Differential component $V_d = V_1 - V_2 = 2A\dfrac{dB}{dt}$: magnetic signal
- Common component $V_c = V_1 + V_2 = 2V_{common}$: unwanted common pickup, e.g., capacitively coupled between probe and plasma

RF ground loop diverting

Chamber side

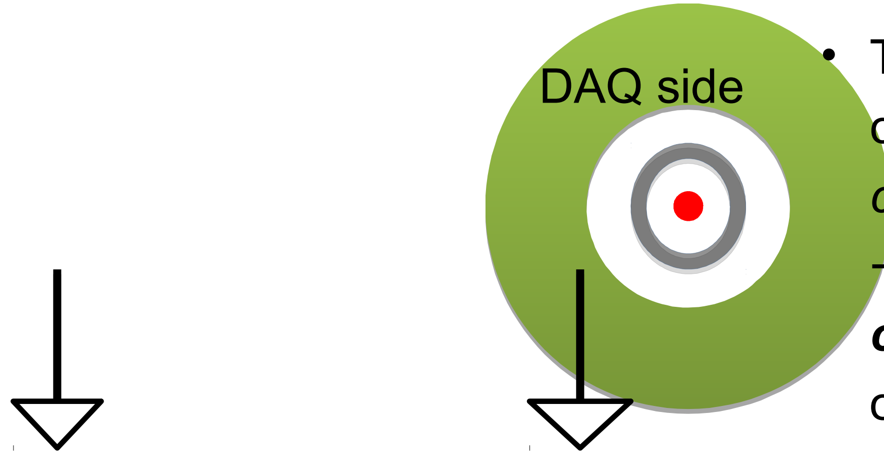

- Thickness of outer conductor of *semi-rigid coax cable* > skin depth → central conductor ***cannot see*** anything outside outer conductor
- But outer conductor ***sees*** large inductance from ferrite core

$$|Z_L| = L\omega$$

$$= 3\Omega \times \frac{L}{100\ \text{nH}} \times \frac{f}{5\ \text{MHz}}$$

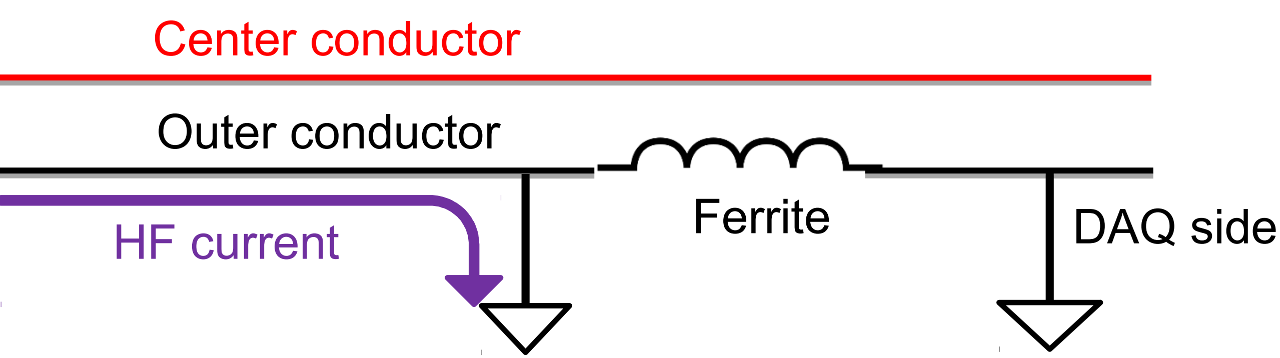

R. J. Perkins and P. M. Bellan, AIP Conf. Proc. **1406**, 531 (2011).

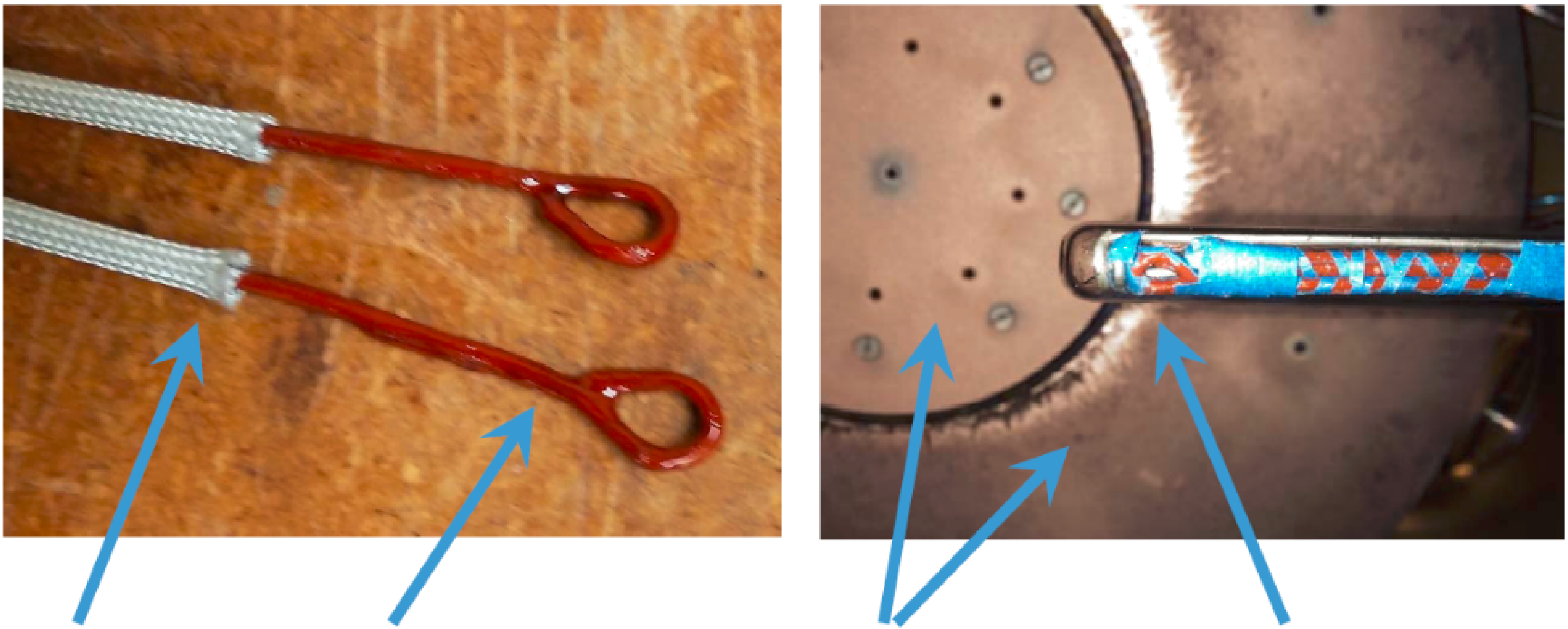

Fiberglass sleeving

Red GLPT insulating varnish

Electrodes

High frequency B-dot probe

Examples of EUV images